Pollution Study 2024, 5(1), 2741.
https://doi.org/10.54517/ps.v5i1.2741

Article

Stochastic dynamics mass spectrometric and Fourier transform infrared spectroscopic structural analyses of composite biodegradable plastics

Bojidarka Ivanova

Analytical Chemistry, Institute of Environmental Research, Faculty of Chemistry and Chemical Biology, University of Dortmund, Otto-Hahn-Straße 6, 44221 Dortmund, North Rhine-Westphalia, Germany; bojidarka.ivanova@yahoo.com, b_ivanova@web.de

CITATION

Ivanova B. Stochastic dynamics mass spectrometric and Fourier transform infrared spectroscopic structural analyses of composite biodegradable plastics. Pollution Study. 2024; 5(1): 2741.
https://doi.org/10.54517/ps.v5i1.2741

ARTICLE INFO

Received: 23 May 2024
Accepted: 3 July 2024
Available online: 22 July 2024

Abstract: The (partial) replacement of synthetic polymers with bioplastics is due to increased production of conventional packaging plastics causing for severe environmental pollution with plastics waste. The bioplastics, however, represent complex mixtures of known and unknown (bio)polymers, fillers, plasticizers, stabilizers, flame retardant, pigments, antioxidants, hydrophobic polymers such as poly(lactic acid), polyethylene, polyesters, glycol, or poly(butylene succinate), and little is known of their chemical safety for both the environment and the human health. Polymerization reactions of bioplastics can produce no intentionally added chemicals to the bulk material, which could be toxic, as well. When polymers are used to food packing, then the latter chemicals could also migrate from the polymer to food. This fact compromises the safety for consumers, as well. The scarce data on chemical safety of bioplastics makes a gap in knowledge of their toxicity to humans and environment. Thus, development of exact analytical protocols for determining chemicals of bioplastics in environmental and food samples as well as packing polymers can only provide warrant for reliable conclusive evidence of their safety for both the human health and the environment. The task is compulsory according to legislation Directives valid to environmental protection, food control, and assessment of the risk to human health. The quantitative and structural determination of analytes is primary research task of analysis of polymers. The methods of mass spectrometry are fruitfully used for these purposes. Methodological development of exact analytical mass spectrometric tools for reliable structural analysis of bioplastics only guarantees their safety, efficacy, and quality to both humans and environment. This study, first, highlights innovative stochastic dynamics equations processing exactly mass spectrometric measurands and, thus, producing exact analyte quantification and 3D molecular and electronic structural analyses. There are determined synthetic polymers such as poly(ethylenglycol), poly(propylene glycol), and polyisoprene as well as biopolymers in bags for foodstuffs made from renewable cellulose and starch, and containing, in total within the 20,416–17,495 chemicals per sample of the composite biopolymers. Advantages of complementary employment in mass spectrometric methods and Fourier transform infrared spectroscopy is highlighted. The study utilizes ultra-high resolution electrospray ionization mass spectrometric and Fourier transform infrared spectroscopic data on biodegradable plastics bags for foodstuffs; high accuracy quantum chemical static methods, molecular dynamics; and chemometrics. There is achieved method performance $|r| = 0.99981$ determining poly(propylene glycol) in bag for foodstuff containing 20,416 species and using stochastic dynamics mass spectrometric formulas. The results highlight their great capability and applicability to the analytical science as well as relevance to both the fundamental research and to the industry.

Keywords: mass spectrometry; stochastic dynamics; biodegradable polymers; quantum chemistry; 3D structural analysis

1. Introduction

Synthetic polymer plastics are widely utilized as packaging materials in a broad spectrum of industrial branches and daily life of humans, mainly due to their low cost, excellent waterproof ability, lightweight, and excellent barrier capability to moisture and oxygen [1]. At about 8.3 billion metric tons of plastic-based materials have been created, so far [2]; and, ca. 6.3 thousand metric tons of corresponding waste has been produced [2].

In total, 9% of plastics waste was recycled. By 2050 at about 12 thousand metric tons of plastics waste shall be cumulated.

Therefore, the increased production of synthetic packaging plastics causes for severe environmental pollution. The elaboration and industrial scale implementation of new biodegradable and renewable bioplastics is of vital importance [1,3].

Biodegradable polymer materials have many different properties and applications [3]. They can be obtained from agricultural sources.

In addition, they be synthesized by monomers or micro-organisms, either biobased materials, or fossils. For instance, starch and cellulose belong to the group of agricultural-based polysaccharides. Poly(lactic acids) is assigned to bio-based polysaccharides. PEG belongs to fossil based petro-sourced biodegradable polymers.

There are major advantages of such plastics compared to conventional polymers. They can save fossil resources via employment in biomass that renews. Bioplastics offer means of recovery at their lifetime end via biodegradability, as well. Over the latter decades, there is increasing in applications of biodegradable polymers; thus, absolutely conditioned by legislative Directives and environmental concerns. The same is valid to products of starch and cellulose. For instance, the aforementioned poly(lactic acid) shows many applications to different industrial branches, including those ones dealing with paper or biofuels production; textile fiber production, replacing synthetic polymers such as nylon and polyester, manufacturing of platform chemicals, and more.

In addition, employment of cellulose from biomass, such as agricultural by-products, is considered to be a green approach to produce biofuels and biochemicals. Biomass is one of the most promising sources of energy, as well. It is the most abundant source of carbon in the environment.

Therefore, biodegradable carbohydrates are particularly prospective materials for industrial scale application to food technologies; medicine; textile innovations, because of wastes from textile and dyeing industries are potential hazards for human life; or to generate green energy. For instance, starch, dextran, and gelatin are used to fabricate 3D biomedical devices for purposes of tissue engineering and reconstruction of organs and scaffolds for stem cells [4,5].

The design, modelling, and improving mechanical and physico-chemical properties of biopolymer; their polymer strength; water resistance; or low water sensitivity is mainly performed via chemical modification of the molecular skeleton of the polymer.

Thus, oxidation of starch or cellulose is one of the most important processes for chemical modification of the biomacromolecules broadly used to textile, paper, and more industrial sectors. Often, OH-groups at C^2-, C^3-, and C^6-positions, are modified

to carboxyl and carbonyl-ones [6].

The (photocatalytic) process, in the latter context, have received tremendous research attention which is due to their environmentally-friendly experimental conditions, cost-effectiveness, and high efficiency. Frequently, they utilise a light-activated semiconductor photocatalyst to generate highly activated (ion)-radicals used not only to degrade pollutant molecules [5,7–12], but also to modify chemically the biopolymers.

Importantly, biodegradable plastics cannot degrade in natural or industrial settings [13].

In addition, consideration of plastics ageing processes to increase relevance of environment is of importance. The ageing reactions of plastics such as polyethylene, poly(lactic acid), and polypropylene, among others, change of material's surface, its chemical properties. There are increased oxygen-containing groups of polymer molecule [14]. The latter fact, increases affinity of plastics toward sorption reactions of metal ions from particular aquatic environmental water.

The major motivation behind replacement of conventional synthetic plastics with biodegradable materials is not only associated with issue of environmental protection from plastics waste, but also with polymerization reactions producing oligomer composite inclusions into polymer material. They are considered as nonintentional added chemicals. In cases when synthetic polymers are used to food packing, oligomers could migrate from polymer packing to food. Thus, there is compromised the safety for the consumers, as well.

The same is valid to many plastics additives. They are not covalently bound to polymer molecular chain. Precursors of N-nitrosamine are used to improve plastics strength and elasticity. However, for instance, the latter analyte itself is potent human carcinogens and mutagens [15].

Therefore, LMWs additives can be released at all stages of lifecycle of polymer materials [16] via migration or via volatilization. The transfer of chemicals from plastic packages to foods, human, and natural environments occurs.

The pure biopolymers are regulated via Directive of the European Union (1935/2004/CEE [17]). Toward additives, there is applied Directive of European Plastics Regulation (10/2011.) It contains a list of authorised chemicals with their specific migration limits [18].

The maximum allowed concentration limits in migration for chemicals which are not explicitly shown [9], must be lower than 0.01 mg kg^{-1} food stimulant or foodstuff.

Therefore, the analytical determining of the latter chemicals should be compulsory done according to the established legislation Directives.

Furthermore, currently, evaluation of materials sustainability often disregarded the effect on human exposure to chemicals [13] when assessing toxicity of new biodegradable materials. Derivatives of biodegradable polymers; for instance, cellulose, are already industrially applied to a broad spectrum of materials. These are dispersants, thickeners, adhesives, emulsifiers, fillers, petrochemical products, ceramics, textiles, synthetic resins, foods, or components in oral pharmaceutics, due to lack of toxicity [19].

However, very little is known of chemical safety of bioplastics, even those

including cellulose and its derivatives. The latter fact makes the discussed gap in knowledge problematic, due to increased application to bioplastics. Scarce research data, so far, have shown that majority of consumer conventional plastics products contain toxic in vitro chemicals [13,16].

The same has been found true for a set of bioplastics [13]. Both the conventional and biodegradable plastics represent complex chemical mixture of known and unknown analytes ranging from polymers, fillers, and additives such as plasticizers, stabilizers, flame retardant, pigments, antioxidants, and more [13,16]. Some of these analytes can be toxic [13].

Therefore, bioplastics have been acknowledged as environmentally friendly materials including lacking toxicity ones. The chemical complexity of packing bioplastic-based materials is equally complex and potentially toxic to both human and environment [20].

Thus, development of safety to human and environmental biodegradable plastics requires research effort in elaboration of new scientific methods and regulatory approaches, including legislation Directives in order to improve their safety manufacturing and applications to humans and the environment.

In the latter context, biomass is highlighted as environmentally friendly, renewable, and carbon-negative source. It is one of the most promising sources of energy, as well [21–23] composed of cellulose, lignin, and hemicellulose. The structural analysis of intermediates of interaction of biomass components is crucial in revealing mechanistic aspects of its chemical reactivity.

Bioplastics are considered more environmentally-sustainable than traditional plastics as, by definition, they are either bio based, biodegradable, or feature both properties. Bio-based plastics limit extraction and use of fossil resources by using biomass; furthermore, biodegradability is an add-on property of certain types of bioplastics which offers additional means of recovery at the product's end-of life and the promotion of a Circular Economy system. There are several bio-based and biodegradable polymers available on the market, such as starch-based bioplastics, poly(lactic acid), polyhydroxy butyrate, polyhydroxyalkanoates, polybutylene adipate therephatlate, and more [24].

Cellulose, is regarded as important biopolymer, amongst others. It has a broad spectrum of applications to many industrial branches and is used to paper products, biofuels production, textile fibers, platform chemicals, etc. [25].

Starch is regarded as promising biopolymer for bioplastics production at an industrial scale, as well. It is a renewable, naturally abundant, biodegradable, and inexpensive material, regarded as promising material for development of eco-friendly bioplastics. It is transferred into thermoplastic derivative in presence of plasticizers such as, for example sorbitol, water, glycerol, etc. However, there is a great challenge to improve mechanical and physico-chemical properties of starch as its polymer strength, water resistance, low water sensitivity, etc. [1,26]. The improvement of its mechanical strength and water resistance is carried out via incorporating hydrophobic polymers such as poly(lactic acid), polyethylene, polyesters, glycols, poly(butylene succinate), and more.

Despite the effort, still bioplastic composite materials do not change significantly the molecular structure, physicochemical properties, and mechanistic

characteristics of starch-based bioplastics; thus, difficulty their competition with synthetic polymers.

However, starch-based bioplastics show stronger mechanical properties comparing with other bioplastics or synthetic polymers. Due to later reasons, enormous research effort is shifted into direction of chemically substituted derivatives of starch [1]. It appears a promising research strategy for elaboration and development of new starch-based functional bioplastics, owing to the fact that there is obtained easily a large number of substituted derivatives from the naturally extracted starch representing dialdehyde carbohydrate derivative [1,26].

Cellulose and starch are most relevant dietary model polymer systems, as well [23,27,28].

In addition, wastewater is generated due to industrial development of plastics, textile, printing, etc. It contains, often heavy metal ions, which compose the environmental metallic pollution, as well. Since, ions of heavy metals are not biodegradable they can be accumulated via the food chain; thus, yielding to (fatal) disorders to human health, including cancers [29]. In this context, development of cellulose-based adsorbents capable of adsorbing ions of heavy metals contribute to remediation and wastewater purification among variety of methods for environmental wastewater treatment. The large number of chemically active hydroxyl groups of the latter biodegradable polymers enhances its adsorption capacity toward heavy metal ions.

Furthermore, there is a large surface area, biodegradable properties, and strong mechanical ones, among many more advantages of composite cellulose polymers [29].

In the context of preceding paragraphs, it becomes clear that the structural analysis is the primary research task of analysis of a polymer. Due to complexity of polymer composites of bioplastics, however, soft-ionization methods for mass spectrometry have been regarded as cornerstone in the field of polymeromics as they are so-called gold-standard of omics-methods of molecular structural analysis of biologically active compounds in vitro and in vivo [30,31]. These approaches are broadly utilized for analyzing biological (macro)molecules; for instance, peptides, proteins, lipids, and carbohydrates, as well [32]. It is governed by superior features and method performances of the analytical mass spectrometry. They have been sketched [30]. The MS methods have become irreplaceable analytical tool in the field of polymer science for purposes of quantitative and structural analyses of such analytes, as well [33]. There are several MS approaches, other analytical methods, and techniques which are fruitfully used for polymers structural determination [3]. The soft-ionization MS methods such as matrix-assisted laser desorption/ionization, electrospray ionization, and atmospheric pressure chemical ionization tools have pioneered the development of new MS-based approaches to polymeromics of synthetic polymers. They replace classical ion sources such as electron impact or chemical ionization, or field desorption, fast atom bombardment ones [34]. The molecular structural analysis of polymers proves not only successful synthesis of polymers, but also detects unexpected side-chain polymer reaction products, including trace amounts of inclusions into the bulk polymer material, having critical health–related implications; thus, being a guarantee of safety, efficacy, and quality.

Therefore, their application to the field of polymer research is the same to this one in omics-methods of biology and medicine.

However, due to complexity of polymer materials there are highlighted limitations to a broad application of MS methods to polymeromics. For instance, (a) the polymer must be capable of stabilizing gas-phase ions; (b) often, conventional MS techniques do not provide specific data on functional groups of polymers or on analyte primary and higher-order molecular structure; and (c) polymeric mixtures could not be determined properly as a result from differences in ionization, respectively, detection efficiencies of polymer material constituents. The following applications of tandem mass spectrometry in polymer research are mainly highlighted: (i) identification and annotation of organic additives in composite polymers, accounting for the fact that the additives are LMWs; (ii) determination of volatile pyrolyzates in polymers; and (3) determination of individual oligomers in LMW polymers [35].

The mass spectrometric m/z measurand of n-mers of a polymer is used to obtain information about molecular weight, compositional heterogeneity, and analyte functionality distributions [36]. Since, the composite materials can be complex analyte mixtures having isobaric analtyes or a mixture of their isomeric 3D structural architectures, then, it can be difficult or even impossible to determine polymers or oligomers in mixtures by single-stage MS measurements of m/z data alone. Thus, for purposes of structural molecular analysis the methods of mass spectrometry mainly use tandem mass spectrometric operation mode.

Although, tandem mass spectrometry often enables compositional identification of carbohydrates, traditional MS/MS fragmentation methods fail to generate abundant cross-ring fragments of intrachain monosaccharides that could reveal carbohydrate connectivity [37].

Particularly, synthetic polymers show three types of tandem MS fragmentation modes: (A) charge-directed path; (B) charge-remote intraionic rearrangements; and (C) charge-remote fragmentation reactions by means of radical intermediates [38], where the latter processes predominate.

In addition, MS surface analysis permits ambient pressure sample measurements; thus, minimalizing the invasive assay of soluble chemicals with an almost lack of sample pre-treatment. There are utilized for the later purposes desorption electrospray ionization and laser ablation electrospray ionization mass spectrometric methods [39].

Despite, currently, there is a lack of universal method for characterization of biodegradable polymers [40].

Nuclear magnetic resonance spectroscopy is also robust method for characterizing polymers. It provides data on repeat molecular structural unit in addition to end-chain groups. The method is capable of revealing specific bonding modes within the chain. It shows low sensitivity; furthermore, it exhibits complex sample preparation steps due to low solubility of analytes as well as complex data-interpretation due to signal overlapping effect. Even, employment in solid state technique of nuclear magnetic resonance is characterized by challenging data-processing tasks, due to effects of peak broadening, time of analysis, and chemical shifts [33,41].

In addition, the latter method requires rather pure samples and lacks the ability to reveal sequence information.

X-ray diffraction is robust analytical method for 3D structural and morphological data on 0.3–0.5 and 1–200 nm scale polymer samples. The beam path scattering variation, due to internal structure of polymers allows for determination of oligomeric or macromolecular polymeric shape and self-organization of the polymer chains. Despite, the weak scattering intensities depending on the type of polymer sample can limit the method's application.

The thermal analytical approaches also find a wide application to polymer science. For instance, differential scanning calorimetry and thermogravimetric analysis are used in polymer characterizations; thus, determining glass transition temperature of polymers, their melting and crystallization temperatures. The thermogravimetric analysis provides data on thermal and oxidative stability of the analytes together with their moisture and volatile contents [33,41].

Fourier transform infrared and Raman spectroscopy is used to determine (bio)plastics, as well [2,42–45]. These spectroscopic methods are routinely utilized for purposes of environmental analysis [5,7–12].

At this point, I would like to make an explicit attempt to sketch that both the vibrational spectroscopic methods and mass spectrometry provide plausible analytical quantitative and structural information about chemicals in complex mixtures. Thus, they are routinely implemented into research on environmental chemistry [5,7–12]. Furthermore, both the MS protocols and vibration spectroscopic ones should be compulsory done within the already developed and established legislation Directives valid to European Union, toward analytical methods and technique for analysis protocols. They are agreed with Council Directive 96/23/EC concerning performance of analytical methods and interpretation of results [46]. The latter reference, particularly, focuses the reader attention on requirements for mass spectrometric and infrared-spectroscopic approaches used to the analytical practice [46].

The question of the advantages of the latter instrumental methods for the purposes of the environmental research is of central importance.

Mostly, vibration measurements can be performed directly on polymer material as well as on fractions isolated from the polymer matrix by solvent extraction or by hydro-distillation. The same is valid to methods of mass spectrometry.

Therefore, the capability of both the vibration spectroscopy and mass spectrometry of analyzing directly complex environmental samples without application to sample-pre-treatment steps appear their crucial advantage, amongst others [5,7–12].

Furthermore, it goes without saying that the latter approaches are applicable to determine both quantitatively and structurally organics, metal-organics, and inorganics pollutants in the environment [5,7–12,47]. For the purposes of the current study, it should be underlined that they are applicable to determine presence of heavy metal ions in the bioplastics. In such cases there is used standards determining inorganics such as EN17033 and ASTMD6400 ones, prescribing maximal concentration limits of heavy metals and organics of high concern in order to ensure environmental protection from hazardous chemicals from biodegradable plastics; if

any. The aforementioned standard treats plastics composted under aerobic environmental conditions in municipal as well as industrial aerobic composting facilities. The developed test method is equivalent to ISO 17088.

Vibration spectroscopy provides characteristic bands of individual components of composite polymer materials. These bands provide data on chemical composition of the samples using, conventional or linearly polarized techniques for data-processing of vibration spectroscopic patterns [48]. However, the approaches are applicable to determine macro components of analytes in the mixtures [48].

In this perspective, the current study shall demonstrate how the aforementioned problems of MS analysis of mixtures of polymers can be bypassed by complementary application of stochastic dynamics model Equations (1) and (2) [49–56] and Arrhenius's Equation (3). Equation (2) is derived from Equation (1) [54].

In addition, it shall evidence the capability of Equation (4) to predict reliably MS spectra of analytes. It is derived on the base on Equations (2) and (3) [47,57,58].

They allow exact mass spectrometric quantitative and 3D molecular structural analysis via quantifying fluctuations of measurable variables per short span of scan time.

$$D_{\mathrm{SD}}^{\mathrm{tot}} = \sum_{i}^{n} D_{\mathrm{SD}}^{i} = \sum_{i}^{n} 1.3194 \times 10^{-17} \times A^{i} \times \frac{\overline{I_i^2} - \left(\overline{I_i}\right)^2}{\left(I_i - \overline{I_i}\right)^2} \quad (1)$$

$$D_{\mathrm{SD}}^{\prime\prime,\mathrm{tot}} = \sum_{i}^{n} \mathrm{D}_{SD}^{\prime\prime,i} = \sum_{i}^{n} 2.6388 \times 10^{-17} \times \left(\overline{I_i^2} - \left(\overline{I_i}\right)^2\right) \quad (2)$$

Equation (2) yields to exact quantitative analysis ($|r|$ = 1), 3D molecular and electronic structure determining when is utilized complementarily with Arrhenius's Equation (3) [49–57]. Function $D^{\cdot\cdot}_{\mathrm{SD}} = f(D_{\mathrm{QC}})$ yields to $|r| = 0.9999_4$, studying LMW analytes [57,58]. The D_{QC} parameter accounts for energy parameters of 3D molecular structure and isotopologies of analyte molecule. The statistical significance of the relation $D^{\cdot\cdot}_{\mathrm{SD}} = f(D_{\mathrm{QC}})$ detailing on 3D molecular structure is assessed via chemometrics.

$$D_{\mathrm{QC}} = \frac{\prod_{i=1}^{3N} \nu_i^0}{\prod_{i=1}^{3N-1} \nu_i^s} \times e^{-\frac{\Delta H^{\#}}{R \times T}} \quad (3)$$

Equation (4) predicts analyte MS spectra using approximations $\langle I^2 \rangle > \langle I \rangle^2$ and $D^{\cdot\cdot}_{\mathrm{SD}} \sim D_{\mathrm{QC}}$. The $I_{\mathrm{SD}}^{\mathrm{Theor}}$ show intensity data on peak of q-th product ion calculated depending on experimental parameters of MS measurements. It does not account for fluctuations of measurands.

$$I_{\mathrm{SD}}^{\mathrm{Theor}} \sim \left(2.6388 \times 10^{-17} \times D_{\mathrm{QC}}\right)^{1/2} \quad (4)$$

Despite, the latter fact, Equation (4) is a simplistic model capable of distinguishing between positional stereoisomers of analytes. Application of Equation (4), so far, has shown $|r| = 0.9992_2$–0.99 correlating theoretical $I^{\mathrm{Theor}}{}_{\mathrm{SD}}$ and experimental $I^{\mathrm{TOT}}{}_{\mathrm{av}}$ data on plant metabolites and alanyl-containing oligopeptides [57,58]. Its application to determine poly(methyl-2-methylpropenoat) composites has shown $|r| = 0.9999_8$ [59].

Herein, Equations (2) and (4) are used to determine biodegradable chemicals in significantly more complex mixtures of composite polymers, determining analytes in

bags for foodstuffs made by polymers based on cellulose and starch as renewable resources. The polymer additives have been authorised for direct food contact and are commercially available marked products. The study uses ultra-high resolution electrospray ionisation mass spectrometry operating in positive polarity, Fourier transform infrared spectroscopy, high accuracy methods of quantum chemistry, and chemometrics, as well.

2. Experimental

2.1. Materials and methods

The study uses experimental datasheets of FT-IR and mass spectra of cellulose samples of bags for foodstuffs Cell_5, Cell_7, and PE_1 as measured and provided by work of Zimmermann et al. [13]. The experimental datasheets are public available and can be downloaded free of charge [60]. There are used experimental mass spectrometric raw files: Cellulose_5.raw, Cellulose_7.raw, and BioPe_1.raw. The sample description is shown in **Table 1**.

Table 1. Plant-based polymer products according to work of Zimmermann et al. [13].

Sample/plastic type	Plastic product	Colour, printing ink	Material information from producer/distributor/vendor
Cell_5	Bag for foodstuff	Transparent, black ink	Composite of cellulose and starch, NatureFlex, made of renewable resources, aroma and oxygen barrier, authorised for direct food contact, all additives are authorised by the FDA and/ or the respective German, Swiss and Austrian Foodstuffs and Commodities Act
Cell_7	Bag for foodstuff	Transparent, white ink	Composite of cellulose (wood) and green PE (sugar cane), made of renewable resources, aroma and oxygen barrier, authorised for direct food contact, all additives are authorised by FDA and/ or the respective German, Swiss and Austrian Foodstuffs and Commodities Act.

Solid-state infrared spectra of film samples within mid-region of the electromagnetic spectrum have been measured on FTIR Perkin Elmer Spectrometer (Waltham, Massachusetts).

The conventional (film) and linearly polarized spectra were recorded within the range 4000–400 cm^{-1} on a Bomem-Michelson 100 FTIR-spectrometer (Bomem Inc., Canada) equipped with a Perkin Elmer wire-grid polarizer with a resolution of ±1 cm^{-1} and 150 scans. The analytical instrumentation has been calibrated according to ISO 9001 quality standards for quality management systems, last reviewed and confirmed in 2021. The International Organization for Standardisation is a world-wide federation of national standards bodies. The analytical instrumentation scheme uses Michelson interferometer operating as Fourier transforms infrared spectrometer. The transmission properties of the polarising beam-splitter (KBr) covers the shown above spectral range. The instrument was evacuated up to P = 0.1 Torr and was used Nd:YAG laser (λ = 1024 nm). The scan speed of the moving mirror was 0.5 cm s^{-1}. Effective sample beam focus image diameter was 0.8 cm. The FTIR analysis of the standards involves the methodology for assessing polymer films by FTIR spectrometry according to ISO 83.080.01 (common requirements for analysing plastics) and ISO 10640 (2011). The calibration of FTIR instrumentation involves

determining of linear dynamic range of the relationship between FTIR-band absorption and analyte concentration of standard samples of polymer mixtures using Beer-Lambert's law. In cases when there is insufficient resolution of the spectroscopic bands, then there is deviation of the aforementioned low. In these cases, there is determined a non-linear calibration pattern within the corresponding concentration region [61]. The data-processing mathematical and statistical methods of FTIR spectroscopic patterns have been detailed on the work of Ivanova et al. [48].

Standard sample of polyethyleneglycol 200 (Sigma Aldrich Inc.) for synthesis was used. There were utilized KBr pellet and film techniques for FT-IR measurements.

Ultra-high performance liquid chromatography coupled to quadruple time-of-flight mass spectrometry/mass spectrometry has been used: Acquity UPLC Waters Liquid Chromatography system and SYNAPT G2-S mass spectrometer (Waters Norge, Oslo, Norway), operating in positive polarity. Two μL CH_3OH extracts (0.15 mg plastic μL^{-1}) have been injected onto a Waters C18 guard column coupled to an Acquity UPLC BEH C18 column (130 Å, 1.7 μm, 2.1 × 150 mm, Waters) with a column temperature of T = 40 °C. The LC flow rate has been 0.2 mL min^{-1} using H_2O with 0.1% HCOOH and CH_3OH with 0.1% HCOOH as mobile phases A and B. The gradient has started with 80%:20% A:B for 0.5 min. Further, it has been increased to 40%:60% at 4.5 min and to 0:100% at 35.5 min. 100% B was maintained until 38.5 min; thus, returning to 20%:80% at 39.5 min and equilibrated for 2 min prior to next injection. The heated ESI(+) source had capillary temperature of 120 °C with a spray voltage of 2.5 kV and a sampling cone voltage of 30 V. The desolation gas flow has been 800 L h^{-1}. The mass spectrometer has been runned in full scan (50–1200 Da) at a resolution of 20000 with a data-independent MSE continuum acquisition with a low collision energy (4 eV) and a high collision energy ramp (15–45 eV). The high-pressure limit was 15000 psi. The injection volume was 2.00 uL. Target column temperature was 40.0 °C. There is a lack of measurements in multiplication [13]. The analytical instrumentation has been calibrated according to ISO 13084 (2018).

Experimental design, sample collection, and analyte extraction can be found comprehensively described [13]. They have been carried out according to recycling standards established by the Society of the Plastics Industry. Each plastics type has been identified by an assigned number. It shows clear connection between the polymer material and its classification within the framework of the recycling system. Consider detail on the work of Villegas-Camacho et al. [62].

2.2. Theory/computations

GAUSSIAN 98, 09; Dalton2011 and Gamess-US [63–66] program packages were used. Ab initio and DFT molecular optimisation were performed by B3PW91 and ωB97X-D methods. The Truhlar's functional M06-2X was utilized. The algorithm by Bernys determines GSs. PES' stationary points were obtained via harmonic vibration analysis. Minima of energy are confirmed when there is a lack of imaginary frequencies of second-derivative matrix. Basis set cc-pVDZ by Dunning, 6-31++G(2d,2p) and quasirelativistic effective core pseudo potentials from Stuttgart-

Dresden(-Bonn) (SDD, SDDAll) were utilized. The ZPE and vibration contributions have been accounted for up to a magnitude value of 0.3 eV. Species in solution were studied by explicit super molecule and mixed approach of micro hydration by PCM. The ionic strengths in solution were accounted for, using IEF-PCM. Merz–Kollman atomic radii and heavy atoms UFF topological models were used. The pH effect was evaluated computing properties in neutral and cationic forms. MD computations were performed by ab initio BOMD was carried out at M062X functional and SDD or cc-pvDZ basis sets, as well as, without to consider periodic boundary condition. The trajectories were integrated using Hessian-based predictor-corrector approach with Hessian updating for each step on BO-PES. The step sizes were 0.3 and 0.25 $amu^{1/2}$Bohr. The trajectory analysis stops when: (a) Centres of mass of a dissociating fragment are different at 15 Bohr, or (b) when number of steps exceed given to as input parameter maximal number of points. The total energy was conserved during computations at least 0.1 kcal mol^{-1}. The computations were performed via fixed trajectory time speed (t = 0.025 fs) starting from initial velocities. The velocity Verlet and Bulirsch–Stoer integration approaches was used.

The Allinger's MM2 force field was utilized [67,68]. The low order torsion terms are accounted for higher priority rather than van der Waals interactions. The method's accuracy is 1.5 kJ mol^{-1} of diamante or 5.71×10^{-4} a.u.

2.3. Chemometrics

Software R4Cal Open Office STATISTICs for Windows 7 was used. Statistical significance was evaluated by *t*-test. Model fit was determined upon by *F*-test. ANOVA tests were used. The nonlinear fitting of MS data was performed via searching Levenberg-Marquardt algorithm [69–74]. Together with ANOVA test, there are used nonparameteric two sample Kolmogorov-Smirnov [75], Wilcoxon-Mann-Whitney [76], and Mood's mediantests [77], as well. ProteoWizard 3.0.11565.0 (2017), mMass 5.0.0, Xcalibur 2.0.7 (Thermo Fischer Scientific Inc.) and AMDIS 2.71 (2012) software were used. The FTIR-spectrometric patterns were processed by means of GRAMS AI 7.0 software (Thermo Fischer Scientific Inc.)

3. Results

3.1. Fourier transform infrared spectrometric data

This sub-section answers to a question: How do we use infrared spectroscopy to determine analytes in composite polymers studying bag for foodstuffs (Cell_5 and Cell_7) in addition to sample Bio-PE_01 containing 85% biodegradable carbohydrate polymer mixture of sugar cane, and additives [13]. The latter sample is 100% recyclable, as well. **Figures 1** and **A1,** in the latter context, depicts FTIR spectra of the studied samples, while **Table 2** summarised their characteristic IR modes together with the data on standard sample of PEG (**Figure A2**). The correlative analysis between the observable IR vibration modes includes analysis of standard frequencies of PE wax according to database, as well.

Despite the fact that samples Cell_5 and Cell_7 is of bags for foodstuffs made by composite of cellulose bioplastics there are markedly different IR-spectroscopic

patterns.

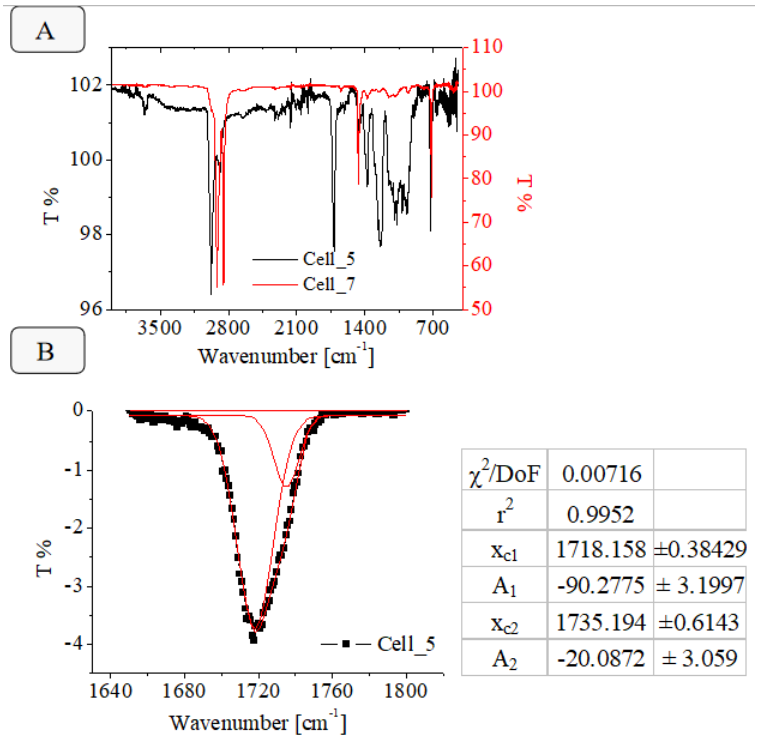

Figure 1. FT-IR spectra of samples Cell_5 and Cell_7 within 4000–500 cm^{-1} in transmission (*T*, %) (A); curve-fitted FT-IR spectrum of Cell_5 sample within 1800–1640 cm^{-1} region of the electromagnetic spectrum (continued as **Figure A3**).

Table 2. Characteristic IR-bands of plant-based polymer products (see **Figures 1** and **A1–A3**).

Sample	**Wavenumber [cm^{-1}]/Assignment**				
	$\nu_{C=O}$	**ν_{C-O}(COOH)**	**ν_{C-H}**	**$\delta_{(O-)C-(C)}$**	**$\gamma_{(C=)C-H}$**
Cell_5	1735.19 ± 0.61		-	-	727.13 ± 0.34
	1718.16 ± 0.38		-	-	735.16 ± 0.72$_{sh}$
Cell_7	-	-	2847.88	1464.58	719.49
			2915.52		729.96 ± 0.20
PE_01			2847.94 ± 0.16	1462.12 ± 0.04	718.95 ± 0.09
			2915.46 ± 0.73		
PEG		1110.11 ± 0.61	2874.11 ± 0.33	1453.88 ± 0.32	956.05 ± 0.33
			2904.02 ± 0.88		

Conversely, samples Cell_7 and Bio-PE_01 show similar IR-spectroscopic modes. The correlation between transmission data on their characteristic IR-modes shows $|r| = 0.9969$. The analysis of sample Cell_7 and PE, respectively, PEG standards yield up to correlation coefficient $|r| = 1$.

Therefore, macro components of Cell_7 are PE and PEG. The IR-spectrum of sample Cell_5 reveals typical for CB-mixtures of cellulose based biodegradable polymers characteristic IR-bands. For instance, the IR-bands at 1730–1720 cm^{-1} belong to $\nu_{C=O}$ stretching vibrations, while the vibration modes at 1150 and 950 cm^{-1} are assigned to ν^{as}_{C-O-C} and ν^{s}_{C-O-C} stretching vibrations of monomeric structural

units of cellulose [78].

3.2. Mass spectrometric data

The MS spectra of sample Cell_5 of composite of cellulose and starch as macro components of polymers is characterised by a set of incorporating hydrophobic polymers such as polyisoprene, polyethylene glycol, and polypropylene (**Figures 2–5**, **B1**, and **B2**.) The shown assignment is according to the common MS fragmentation schemes of synthetic polymers have been proposed by Jackson and co-workers [79–81] as well as Lattimer and Wesdemiotis and co-workers [35,38,82–86]. **Figures 6** and **B3** depict chemical diagrams of characteristic MS parent and product ions of polymers accounting for both the linear and macrocyclic molecular structures of the species.

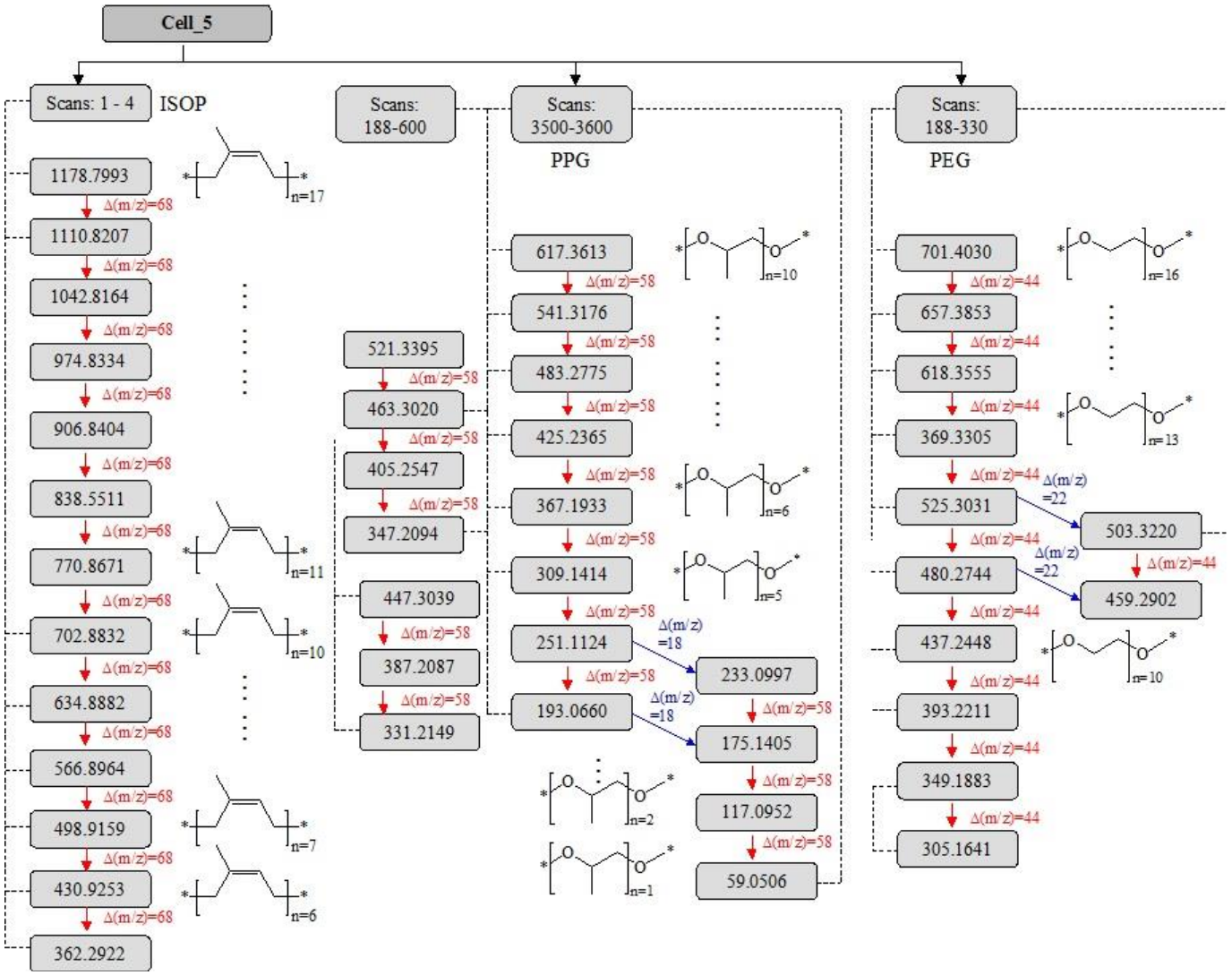

Figure 2. Mass spectrometric data on oligomer species of species in sample Cell_5 with respect to different short spans of scan time; chemical diagrams of cations.

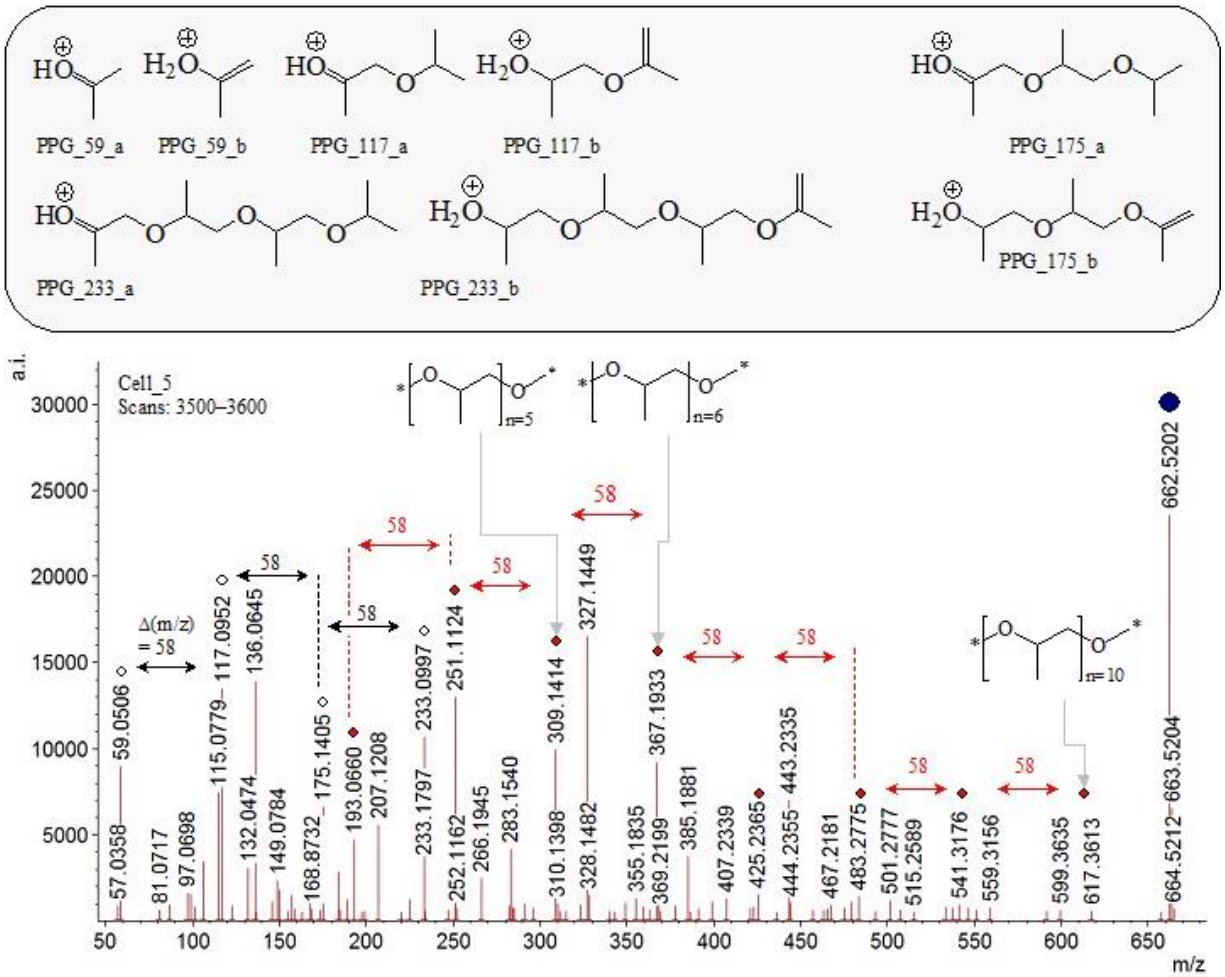

Figure 3. Mass spectrum of sample Cell_5 over short span of scan time 40.35–40.93 mins and scan numbers 3500–3555; characteristic mass spectrometric peaks of PPG; chemical diagrams of observable ions of PPG at m/z 233, 175, 117, and 59 accounting for their different protomers.

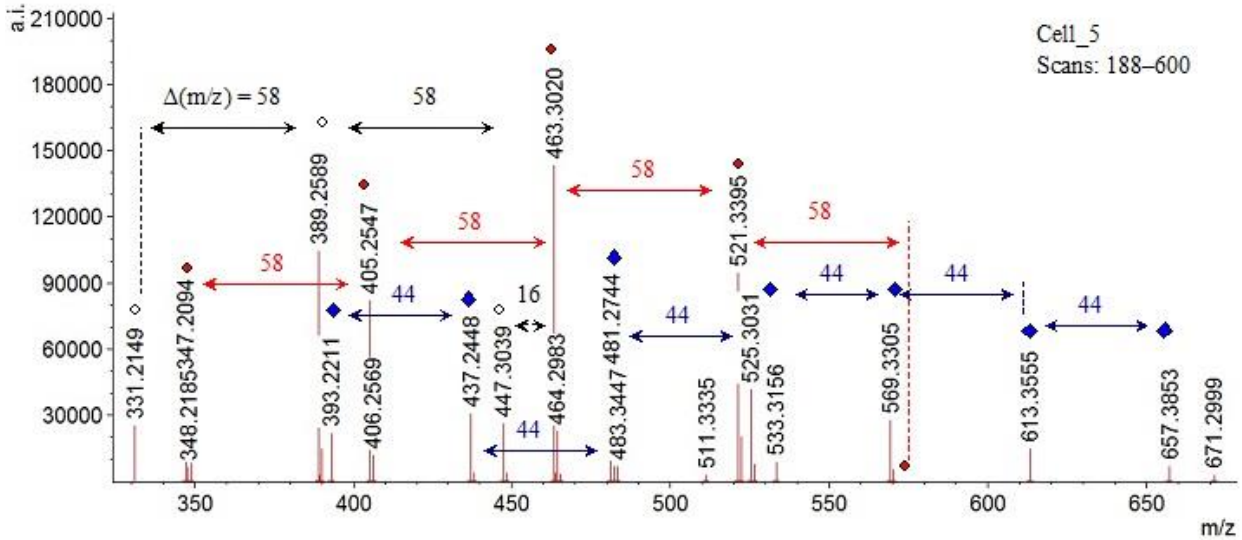

Figure 4. Mass spectrum of sample Cell_5 within scan numbers 188–600.

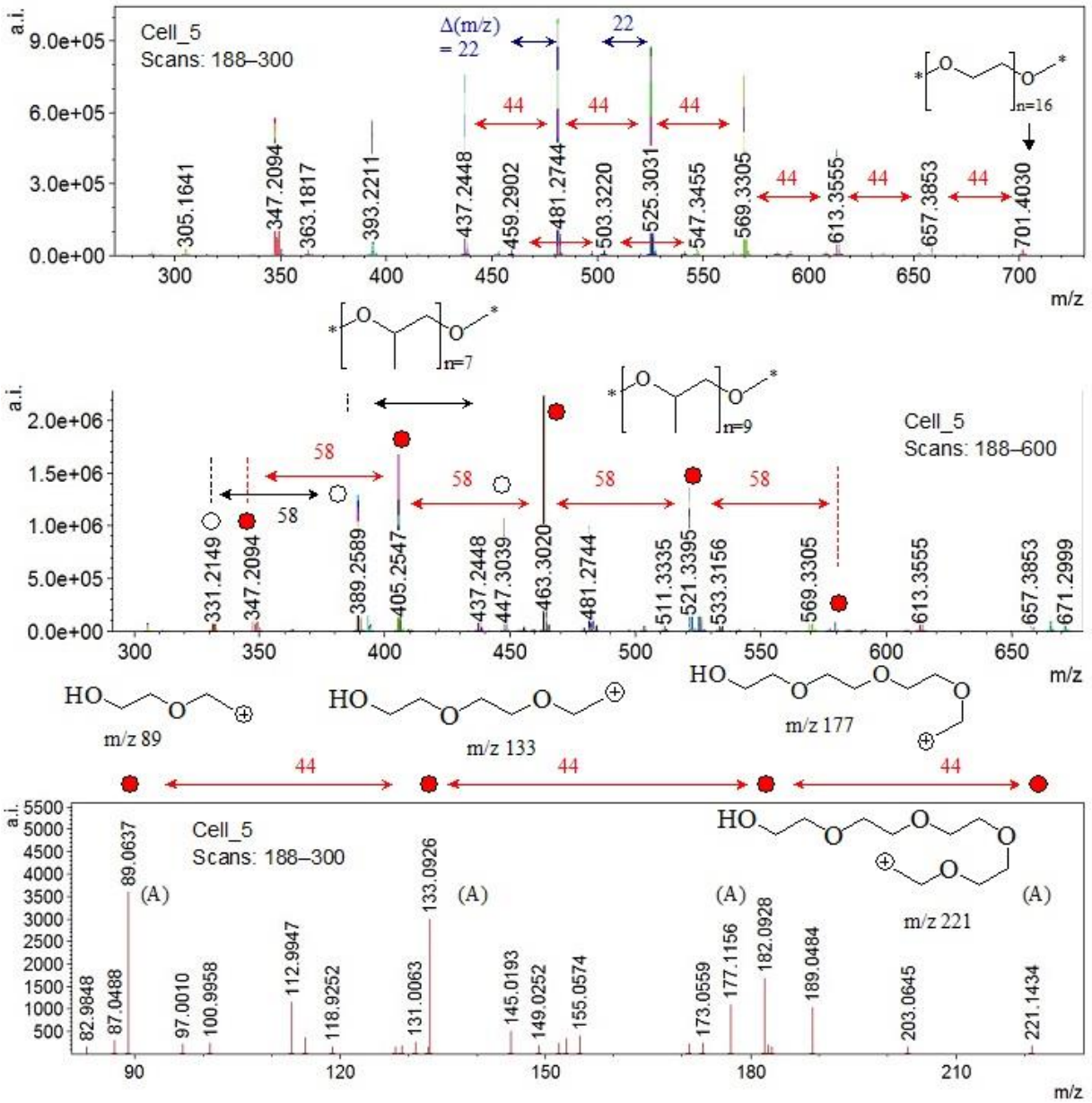

Figure 5. Mass spectrum of sample Cell_5 over short span of scan time 4.76–5.96 mins and scan numbers 188–300; characteristic mass spectrometric peaks of PEG and PPG; chemical diagrams of observable ions of PEG at m/z 221, 177, 133, and 89, respectively.

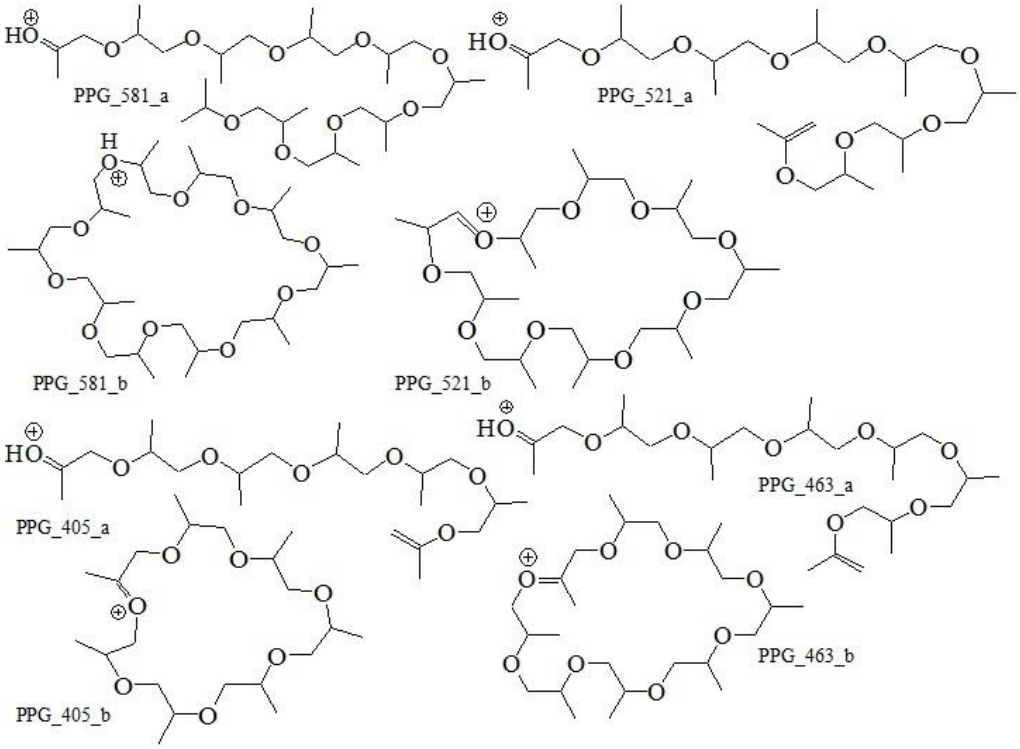

Figure 6. Chemical diagrams of observable mass spectrometric ions of PPG accounting for proton accepting position.

The MS peaks at m/z 1178.7993, 1110.8207, 1042.8164, 974.8334, 906.8404, 838.8511, 770.8671, 702.8832, 634.8882, 566.8964, 498.9159, 430.9253, and 362.9322 show peak spacing Δ(m/z) = 68. The mass spectrum of 11 isoprene units shows peak at m/z 775.7 of $[M + Li]^+$ cation [87]. The product peaks show spacing Δ(m/z) = 68.

Thus, MS spectrum of Cell_5 (scans 1–4) is assigned to inclusion of ISOP, due to the fact that there are observed MS ions at m/z 1178.7993, 1110.8207, 1042, 8164, 974.8334, 906.8404, 838.8511, 770.8671, 702.8832, 634.8882, 566.8964, 498.9159, 430.9253, and 362.9322, respectively. The peak spacing is Δ(m/z) = 68. The MS peak at m/z 702.8832 in sample Cell_5 is assigned to oligomer of ten isoprene units stabilized as NH_4^+-adduct. The theoretical value is 702.69167. **Figure B2** depicts 2D chemical diagrams of addicts of product ions of oligomers of polyisoprene, determined in sample Cell_5.

The MS peaks at m/z 579.3818, 521.3395, 463.3020, 405.2547, and 347.2094 having spacing Δ(m/z) = 58 of oligomer poly(propylene glycol) [88].

Since, analyte PPG is an oxygen rich polymer, it is often ionized by Na^+-adduction thus producing cation of sodium adduct, as well. The theoretical data involves both linear and cyclic oligomer (so-called crown ethers) and linear (hydroxyl- or methyl-terminated) oligomer units of the synthetic polymers [35,84].

Copolymers containing poly(ethylene oxide) are an important component in a variety of commercial and household products. PEO and PPO copolymers find applications as plasticizers, lubricants and wetting or dispersing agents in textile, leather, and paper and rubber industries [86]. They are, often used to surfactants and engineering plastics. The mass spectra of random PEO/PPO copolymers are characterised by peak spacing Δ(m/z) = 44 [38,86].

In addition, MS peak spacing Δ(m/z) = 44 is observed in case of standard dimethyl terminated PEO [38] showing two homologous series of product ions, i.e., C_n" of methoxy/hydroxyl end groups and b_n one of methoxy/vinyl end groups. Thus, peak spacing Δ(m/z) = 44 is found in PEGs and PEOs [3]. There is observed loss of 44 + 58 from precursor ion, in addition to loss of 44 + 32 Da [38]. There are observed also product ions with variety of end groups such as dihydroxy (J_n^{HH} ions); hydroxy/vinyl (J_n^{HV} ions), carbonyl/hydroxy (J_n^{CH} ions), and ethyl/vinyl (J_n^{EV} ions), respectively [38]. The fragment species of type J_n^{CE} and J_n^{HV} are isomers.

The same is valid to PEG showing mass spectra having peak spacing Δ(m/z) = 44, due to repeat only ethylene oxide units [35,85,89,90]. The m/z range within 50–500 of PEGDME is characterized by product ions of CID-MS/MS measurements of cation at m/z 487 at m/z 323, 279, 235, 221, 191, 177, 161, 147, 133, 117, 103, 89, 73, and 59, while PEGME shows species of CID-MS/MS (m/z 517) reactions at m/z 265, 235, 221, 191, 177, 175, 161, 147, 133, 131, 117, 103, 89, 87, 73, 59, and 45 [35]. The former analyte reveals three ions series which are spaced with Δ(m/z) = 14. The non-substituted PEG reveals product peaks of CID-MS/MS (m/z 459) within the latter region at m/z 441, 415, 397, 371, 353, 327, 309, 283, 265, 239, 221, 133, 89, and 45, respectively. As can be seen there is significantly complicated patterns of the latter analytes; furthermore, showing a set of common characteristic product ions, which difficult significantly their unambiguous assignment. The structural determination is particularly complicated in case of mixtures of these analytes with biodegradable polymers of carbohydrates, due to a set of common product ions (below).

Despite, quantitative MS analysis of mixtures of the aforementioned analytes have shown that they can be accurately determined (r^2 = 0.998) examining the absolute intensity ratios of their characteristic product ions [91]. The same approach applied to quantify PPGs in mixture has shown r^2 = 0.9982–0.9987 [92].

Furthermore, PEGs have been comprehensively examined from perspective of molecular structural analysis systematising the following series of species. There are series of ions A: CH_3-O-(-C_2H_4-O-)$_n$-H 'methyl ether', B: C_2H_5-O-(-C_2H_4-O-)$_n$-CH_2-CHO 'ethyl ether/aldehyde'; C: CH_3-O-(-C_2H_4-O-)$_n$-C_2H_5 'methyl-ethyl ether'; D: C_2H_5-O-(-C_2H_4-O-)$_n$-H 'ethyl ether'; and E: C_2H_5-O-(-C_2H_4-O-)$_n$-C_2H_5 'diethyl ether', respectively [85]. For instance, common ions at m/z 89, 133, 177 and 221 belong to series (A) of species. Ions at m/z 235 and 161 belong to (B) and (C) series. The product ion of PEG at m/z 239 is assigned to (E) structural series, while ions at m/z 131 and 175 of PEGME—to (D) series of ions.

Thus, as **Figure 5** reveals the MS peaks of Cell_5 samples (scans 188–300) at m/z 89.0637, 133.0926, 177.1156, and 221.1434 having peak spacing Δ(m/z) = 44 is assigned to (A) series of PEG ions [35,85] of type HO-(C_2H_4-O)$_n$-$CH_2CH_2^+$.

Besides, Glc-di- and oligosaccharide fragmentation ions shown above, the Cell_5 sample reveals abundance MS ion at m/z 679.4475 and 622.6202 belonging to hexose-acid and oxo-Glc4 tetramers. The loss of Δ(m/z) = 162 monomer units from the latter species causes for peaks of product ions at m/z 515, 355, and 193 as well as at m/z 501 and 340 assigned to corresponding trimers, dimers, and monomers of the shows species (**Figures 7** and **B4**).

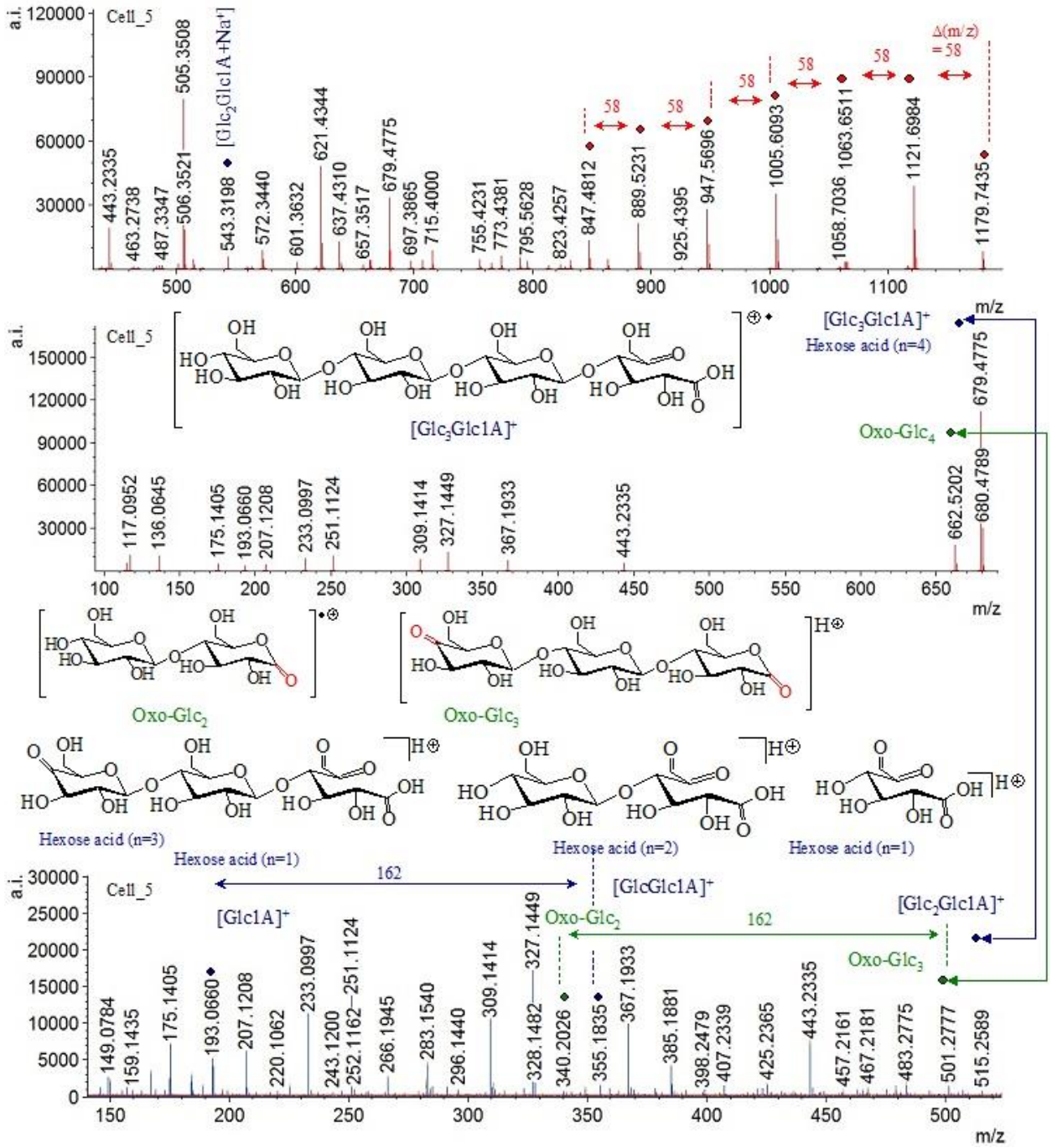

Figure 7. Mass spectrum of sample Cell_5 over short span of scan time 4.76–5.96 mins and scan numbers 188–300; characteristic mass spectrometric peaks of carbohydrate; chemical diagrams of observable carbohydrate ions.

Analogous MS data have been comprehensively analysed studying oxidation products of D-glucose oligomers [93,94]. As **Figure B4** reveals, peaks at m/z 193.066 (Y_1), 220.1062 ($^{2,4}A_2$), 266.1945 ($^{0,2}A_2$-H_2O), 355.1835 (Y_2), and 385.1880 ($^{2,4}A_3$) together with aforementioned ones of protomers and sodium adduct of acidic form of cellotriose (β-D-glucopyranosyl-(1→4)- β-D-glucopyranosy-(1→4)-D-glucopyranose) agree excellent with previously reported results from standard samples of the discussed CBs [93,94]. Due to these reasons, the assignment of the product species is performed in agreement with the latter works.

In examining cellotetraose standard samples having only one β-(1→3)-linkage

at varying position, there has been found that the intensity data on product ions of the oligomer at m/z 655.21, 503.16 (C_3), 443.14 ($^{0,2}A_3$), 341.11 (C_2), 323.10 (C^2-H_2O), 179.06 (C^1), and 161.05 (C^1-H_2O) depends on the isomeric forms: furthermore, distinguishable [93]. The peak at m/z 443.14 is characteristic one for only terminally β-(1→3)-linked oligomer (G1→^{3}G1→^{4}G1→^{4}G). The same is valid to peak at m/z 323.10 assigned to C^2-H_2O product ions. The correlation between intensity ratios of the latter oligomer ions shows $|r| = 0.9829 - 0.5417$ (**Figure B5**). The data agree well with results from MS analysis of cellotriose [95] examining peaks at m/z 503, 341, and 179 showing mutual correlation of the intensity parameters of $|r| = 0.99878$, while the correlation between data on cellotriose and stachyose looking at the latter peaks shows $|r| = 0.7188_4$. As work of Dallinga and Heerma [95] comprehensively discusses the cellotriose and stachyose carbohydrates show a set of common product ions at m/z 503, 443, 425, 383, 341, 283/281, and 121. The mutual correlation between data on the latter CBs yields to $|r| = 0.4622_6$. The MS/MS data on the characteristic peak at m/z 221 of the latter two CBs produce product ions at m/z 203, 189, 161, 159, 131, 119, 113, 101, 89, and 71, respectively. Correlative analysis of these MS/MS data on analytes shows $|r| = 0.8685_4$.

Thus, despite, the visually similar m/z measurands of cellotriose and stachyose carbohydrates the intensity data of the observed peaks are significantly distinguishable from perspective of chemometrics. Due to these reasons, the aforementioned MS peaks of the cellulose tetramer of Cell_5 sample have been examined via Equations (2)–(4) in order to correlate the data on the biodegradable plastic mixture and standard samples.

Within the low m/z values Cell_7 sample reveal a set of characteristic MS peaks at m/z 150, 144, 142, 126, 120, 119, 115, 114, 107, 98, 97, 96, 89, 84, 72, 71, 70, 68, and 43 [21] of carbohydrates (**Figure B6**), despite the fact that there is PEG/PPG based polymer macro components according to the FT-IR data on the preceding sub-section. Furthermore, there is complex mixture of different oxidised products of cellulose together with their (di) anhydrous-derivatives (**Figures 8, 9** and **B7**).

Data on cellulose and hemicellulose show within low m/z values as can be expected several similar fragmentation patterns showing peaks at m/z 217, 201, 185, 163, 151, 139, 127, 111, 97, 83, 64, and 57 (cellulose) as well as at m/z 205, 191, 177, 167, 153, 139, 125, 111, 94, 81, 69, 55, and 44 (hemicellulose) [96]. MS peaks at m/z 163, 162, 145, 133, 126, 119, 115, 102, 97, 91, and 85 are, particularly, associated with product ions of 3,6-anhydro-D-glucose [97,98]. The MS peak at 114 is highlighted as characteristic one of cellulose degradation reactions, while the ion at m/z 144 is assigned to 1,4;3,6-dianhydro-glucopyranose [99].

Mass spectrometric data on starch and cellulose standard samples in negative polarity show abundance MS peaks having spacing Δ(m/z) = 162 at 1295.4191, 1133.36, 971.31, 809.26, and 647.2, respectively [27]. The common ion at m/z 485.15 is doubly charged in the former CBs, while it is monocation of MS spectrum of cellulose. Starch is characterised by two additional dicationic MS peaks at m/z 323.61 and 242.58.

Thus, characteristic MS ions at m/z 175, 159, 143, 127, and 95 have been

observed and assigned studying anhydrous-hexoses [98], particularly underlying the fact that MS peak at m/z 103 and 101 are typically found in mass spectra of methylated anhydrous-hexosides. Disaccharide product ions of 3,6-anhydro-L-galactosyl-D-galactose have been identified due to mass spectrometric spacing of m/z 306.06 [100]. The corresponding monosaccharide units of the latter species are characterized by peaks at m/z 144.04 and 180.04. Importantly, characteristic MS ion at m/z 180 is found in lignin mass spectra, as well [99].

Cell_7 sample is characterised by abundance MS peaks at m/z 705.5122 and 546.4894 having spacing Δ(m/z) = 160. They can be assigned to C^1-oxidized oligosaccharides (m/z + 16) looking at a comprehensive analysis of oxidation reactions of cellulose [101]. There has been shown that observable MS peaks at m/z 705.2236 and 543.0605 are assigned to sodium adducts of $[DP4 + 16 + Na]^+$ and $[DP3 + 16 + Na]^+$ ions. **Figures 8** and **B6** depict the MS spectra and chemical diagrams of the discussed species. Despite, the MS peak at m/z 705 has been assigned to C4-gem-diol of the cellulose tetrameter, as well [102,103]. The observed MS fragments pattern indicates, rather, a co-existence of different oxidised forms of cellulose oligomers, including a gem-diol one as well as aldonic acid form at the reducing end. Non-oxidised fragment species of cellulose are also observed.

Therefore, the observable MS pattern of sample Cell_7 within 3500–3515 scans can be assigned to geminal diol of cellotetrose oligomer as followings: m/z 727.4974 ($[M_4 + Na]^+$), 507.2461 (B_3/Z_3-H_2O), 467.2181 ($^{2,4}X_2$ or $^{2,5}A_3$), 453.2308 ($^{3,5}A_3$ or $^{0,3}X_2/^{1,4}A_3$), ad 365.1552 (Y_2), which is in agreement with data on [103]. In parallel, the C1-oxidized product of cellulose oligomers are assigned to disoddium adducts, as well as followings: m/z 727.4974 ($[M_4 + 2Na\text{-}H]^+$), 709.21 ($[M_4 + 2Na\text{-}H_2O]^+$), 565.3593 ($Y_3$), 551.5090 ($^{2,4}A_4$-$H_2O$), 529.4725 ($C_3$), 509.1532 ($B_3$), 467.2181 ($^{0,2}A_3$), 402.5182 ($Y_2$), 365.1639 ($C_2$), and 304.8507 ($^{0,2}A_2$), respectively. The latter assignment agrees with results from MS analysis of C^1-oxidized cellulose oligomers, as well [103]. MS peaks at m/z 707and 365 have been assigned to sodium adducts of dimer ad monomer of cellobiose, as well [39]. Importantly, identification and annotation of C^1-, C^4-, and C^6-oxidised CBs does not represent a straightforward task. Despite, various analytical methods have been developed for such as purposes [104].

Particularly, challenging is the determination of C^1- or C^4- or both of these oxidation products of cellulose oligomers due to their elution times [104]. The same is valid to employ MALDI-MS/MS, despite, the superior method performances. The determination of only m/z data does not capable of distinguishing between C^1- and C^4-oxidised oligosaccharides: thus, highlighting the research task as far from easy one [104].

The oxidation of C^1-centre of CBs causes for forming of labile δ-lactones; thus, further producing in water aldonic acids [103–108]. These analytes can be well separated by high performance anion exchange chromatography.

Conversely, C^4-oxidation reactions of CBs produce 4-ketoaldoses leading to hydrates or geminal diols. C^4-oxidized oligosaccharides undergo tautomerization in alkaline conditions and that limits their analysis by commonly used high performance anion exchange chromatography. However, there has been questioned

whether double oxidised cellulose products are C^1/C^4 oxidised, or C^1/C^6 oxidised ones, as suggested elsewhere [108].

As has been highlighted [104] MS cannot distinguish high performance anion exchange chromatography isomers and geminal diol form of corresponding C^4-oxidised products of the same oligosaccharide. The C^1-oxidised CBs have the same m/z values [104]. To overcome these challenges there is often used chromatography coupled to mass spectrometry. Despite, there is a lack of a systematic analysis of MS/MS fragmentation patterns of different separated via chromatoraphy C^1- and C^4-oxidised CBs [104,109,110]. The identification of these C^1- and C^4-oxidised carbohydrate structures is far from straightforward, albeit various analytical approaches have been developed as thoroughly reviewed previously.

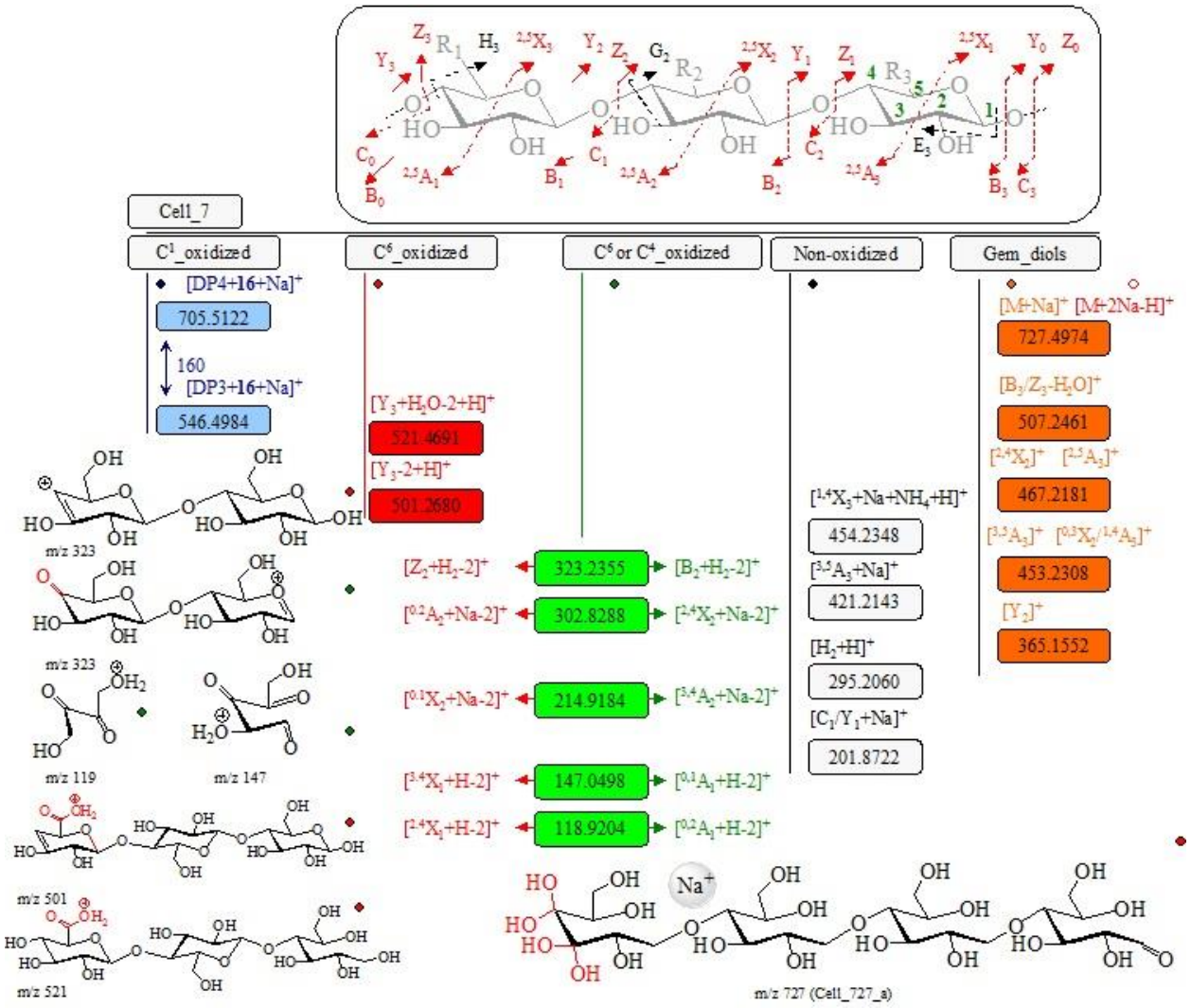

Figure 8. Mass spectrometric data on oligomer species of cellulose and its oxidised products in sample Cell_7; chemical diagram of the cations; fragmentation ion mass spectrometric pattern and assignment of carbohydrate ions is carried out using the nomenclature by Dommon and Costello [111], Stephens and co-workers [112], as well as, Spina and co-workers [113].

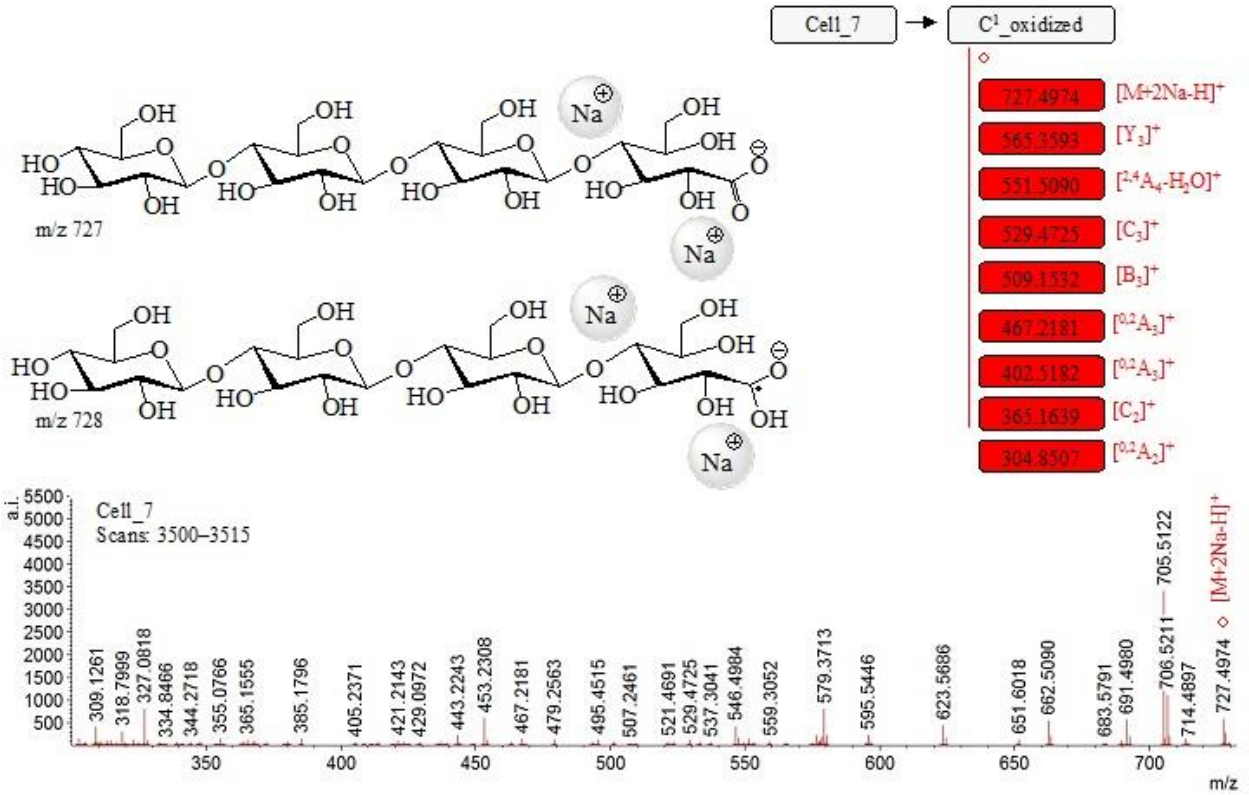

Figure 9. Mass spectrum of sample Cell_7 over short span of scan time 40.09–40.23 mins and scan numbers 3500–3515; characteristic mass spectrometric peaks of C^1-oxidized carbohydrate, assigned according to the nomenclature by Dommon and Costello [111], Stephens and co-workers [112], as well as, Spina and co-workers [113]; chemical diagrams of ions at m/z 727 and 728.

3.3. Theoretical data

The suggestions of works [47,49–58] provide an approach to justify the linear correlation between experimental stochastic dynamics $D^{"}_{SD}$ parameters of Equation (2) reflecting the measurable variable intensity of parent and product peaks of analyte together with the fluctuations of the measurand and theoretical D_{QC} parameter of Equation (3) as test which statistical significance is evaluated by methods for chemometrics as criterion on reliable assignment of experimental MS peaks to corresponding 3D molecular and electronic structures of analytes.

However, when it comes to application of Equation (3) for purposes of 3D molecular structural analysis there is a challenging research task, since the D_{QC} parameter is calculated using vibration modes of species in their ground and transition states.

Despite, the fact that there are already used routine computational tools for purposes of ground and transition states vibration analysis, whether we are assessing claims about 3D molecular structural assignment of experimental measurable variables to corresponding 3D molecular conformations and electronic structures, we need independent computations of a set of proposed molecular models in order to increase the reliability of the structural analysis. As **Figures 6** and **B3** show in cases of PEG and PPG product ions of oligomers there is accounted not only for the proton accepting centre of the mass spectrometric ion, but also for its linear and macrocyclic 3D configurations.

In addition, it is commonly supposed that there should be assessed the proton accepting capability of the O-centres of the later species with increasing in the number of oligomer, respectively, polymeric product ions of the analytes at large m/z-values.

As can be seen, the structural assignment of MS species of polymers within the framework of linear relationship $D^{"}_{SD} = f(D_{QC})$ includes a large number of probabilistic associations, which, however should be certainly utilised for figuring out reliable assignment of the observable MS peaks to corresponding 3D molecular conformation and electronic structure of parent and product ions.

The application of the discussed innovative approach to determine molecular structures of analytes mass spectrometricaly, so far, has shown that Equation (2) is not only correct one, but an exact model for data-processing of measurable variables. In examining oligomers and polymers of aliphatic species both the linear and macrocyclic molecular models there is a significantly flexible molecular skeleton allowing to stabilise a set of closely disposed as energetic 3D molecular conformations. For short chain oligomer candidate species, the computational tasks are exceedingly easy.

However, with increasing in polymer chain, there is increasing in number of computations of species depending on proton accepting positions of cations and their 3D molecular conformations. Thus, we might hope that the complementary application of static and molecular dynamics data at various level of theoretical accuracy there shall be provided the unique geometry parameters of MS molecular ions corresponding to global minimum of energy, respectively, saddle point of transition states.

Clearly, the amount of theoretical data on oligomers and polymers of the studied compounds needed to make reliable use of parameters of Equation (3) may seem overwhelming. In such cases what could justify assumptions that parameters $D^{"}_{SD}$ and D_{QC} of an examined set of models of large oligomer or polymeric MS ions are functionally dependent on each other is assessment of the coefficient of linear correlation between the discussed parameters of Equations (2) and (3) within the framework of a large and statistically representative set of species, their protomers, respectively 3D molecular conformations. As can be expected, with increasing in statistical representatives of examined models there is increasing in reliability of 3D molecular structural assignment of the species to their corresponding experimentally observable MS peaks.

The need of this kind of theoretical analysis which lacks of an alternative that looks more-or-less less complicated is motivated with the fact that composites of biodegradable polymers are characterised not only with a large number of oligomers and polymers in addition to LMWs as preceding sub-sections already have illustrated, but also the MS peaks of the large number of structurally very similar polymers produce virtually identical MS patterns, which structural assignment as highlighted above does not represent a trivial research task. Within the framework of the probabilistic theory the theoretical design of the computational tasks should provide good reason to be confident that a statistically representative set of molecular species is accounted for in evaluating the statistical significance of the correlation between parameters of Equations (2) and (3).

Owing to what I am pointing to, let us look at results from molecular dynamics computations of species of PPG oligomers at m/z 233, 175, 117, and 59 observed within scan time 40.35–40.43 mins of sample Cell_5 (**Figure B8**). There are studied different types of protomers at M062X/SDD level of theory as **Figure 3** (above) has already shown. **Table C1** summarises energetics of species, while **Tables C2** and **C3** their atomic co-ordinates and frequency modes in ground and transition states. **Figure C1** depicts static and molecular dynamics data on species.

Computational data on species of PEG are shown in **Figure 10**. Most stable appear OH^+-protonated macrocyclic cations comparing with corresponding linear molecular ions.

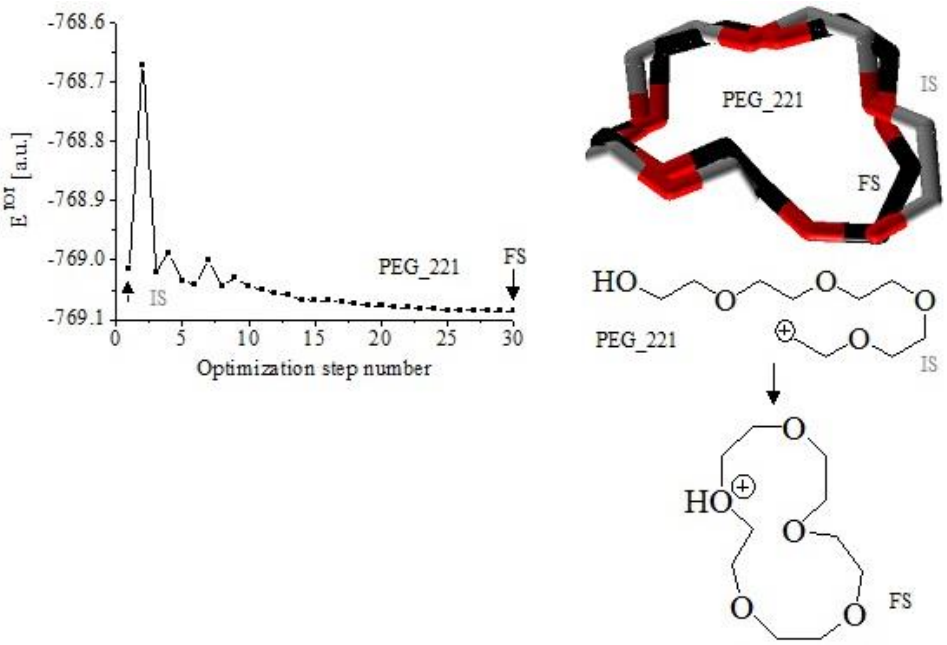

Figure 10. Ionic (M062X/SDD) optimisation of cation at m/z 221 of PEG: Total energy (E^{TOT} [a.u.]) with respect to optimisation step number; chemical diagrams of ions in initial (IS) and final (FS) states; optimised 3D molecular geometry of the PEG_221 ion in its final state; 3D MM2/MD geometry of PEG_221 cation in initial state.

3.4. Correlative analysis between experimental and theoretical mass spectrometric data

In this subsection I should like to argue that a reliable assignment of observable MS peas to corresponding 3D molecular and electronic structures of oligomer product ions of polymers we find in model Equations (2) and (3) and assessment via chemometrics of functional relationship of their parameters examining relation $D^{"}_{SD} = f(D_{QC})$. In studying data on product ions of PPG as **Figure 11** reveals there is achieved excellent to exact chemometrics parameters $|r| = 0.9998_1 - 0.9913_8$ using both relationships $D^{"}_{SD} = f(D_{QC})$ of data on Equations (2) and (3) as well as Equation (4). The latter figure correlated theoretical and experimental data on species as they are listed in **Tables C1** and **C4**.

From the obtained results depicted in the latter figure under consideration we assign the MS peaks at m/z 59.05063, 117.04517, and 175.1405 of PPG to the following 3D molecular and electronic structures of protonomers, i.e., PPG_59_b,

PPG_117_a, and PPG_175_b, due to obtained parameter best |*r*|-parameter. The assignment of MS ion at m/z 233.0973 to protomer PPG_233_a yields to |*r*| = 0.9158_1—a higher value, comparing with this one of a relationship involving data on protomer PPG_233_b. The functional relation $D^{\cdot\cdot}_{SD} = f(D_{QC})$ accounting for the discussed data on the four MS ions as their highlighted most reliable assignment yields to |*r*| = 0.90613.

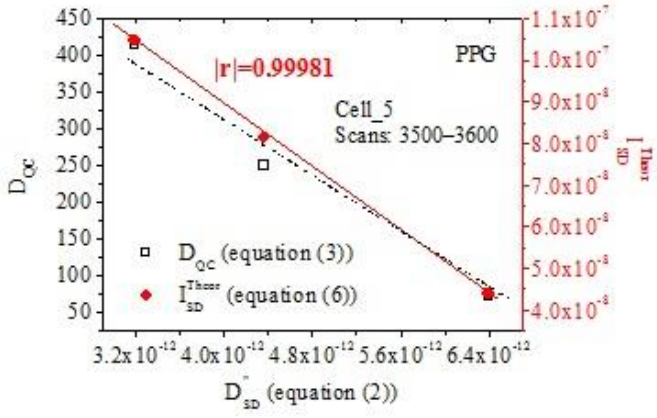

$D^{\cdot\cdot}_{SD}=f(I^{Theor}_{SD})$

Parameter	Value	Error	
A	$1.33805.10^{-7}$	$2.13875.10^{-8}$	
B	-11582.36725	3591.5325	
|r|	sd(yEr±)	N	*p*
0.91581	$1.44628.10^{-8}$	4	0.08419
Parameter	Value	Error	
A	$1.64484.10^{-7}$	$1.77881.10^{-9}$	
B	-18904.5312	367.99439	
|r|	sd(yEr±)	N	*p*
0.99981	$8.4414.10^{-10}$	3	0.01239

$D^{\cdot\cdot}_{SD}=f(D_{QC})$

Parameter	Value	Error	
A	560.32224	124.76544	
B	$-6.34733.10^{13}$	$2.09514.10^{13}$	
|r|	sd(yEr±)	N	*p*
0.90613	84.36968	4	0.09387
Parameter	Value	Error	
A	732.99336	66.86224	
B	$-1.04685.10^{14}$	$1.38322.10^{13}$	
|r|	sd(yEr±)	N	*p*
0.99138	31.72964	3	0.08363

Figure 11. Functional relation between $D^{\cdot\cdot}_{SD}$ and D_{QC} parameters of Equations (2) and (3) as well as experimental average intensity data on characteristic mass spectrometric peaks and theoretical intensity values I^{Theor}_{SD} of Equation (4) looking at ions of PPG in Cell_5 sample; chemometrics.

The excellent-to-exact performances assume theorising under discussion about Equations (2)–(4). It establishes facts about a statistically significant to exact linear relation between experimentally intensity parameter of MS peak and its fluctuations over a short spans of scan time and unique 3D molecular and electronic structure of analyte ions.

Furthermore, the relation accounts for a set of structurally similar polymers and their possible product ions of mass spectrometric fragmentation.

We need to make detailed assumptions about 3D molecular conformation and electronic structure of species on the base on quantum chemical computations of energetics of ions matched to highly reproducible and ultra-high accurate experimental measurable variables. The design of Equation (2) and its functional relations with Equation (3) or (4) ensure validity of our statement and reliability of the structural analysis, due to use to quantitative criteria of chemomerics.

Therefore, the value |*r*| = 0.9998_1 of relation $D^{\cdot\cdot}_{SD} = f(D_{QC})$ of shown product ions of PPG oligomers assumes a highly reliable assignment of observed MS peaks of polymer product ions to the presented 3D molecular and electronic structures of the species.

4. Discussion

Developing the innovative stochastic dynamics mass spectrometric approach to determine exactly quantitative and 3D structurally chemicals in environmental and food samples as well as biological fluids; thus, highlighting its great application to determine polymers in biodegradable plastics would require, first, underlying strength of Equations (1), (2), and (4) as a whole.

However, this task cannot be accomplished in the current paper.

Thus, I shall for purposes of this study, instead of briefly focus the reader's attention on some basic aspects as an effort to underline novelty, advantages, limitations, and applications to both fundamental research and industry. My discussion should be to lay out features which make stochastic dynamics mass spectrometry attractive concept not only for studying (bio)polymers, but also for interdisciplinary fields of the analytical research. However, all they are connected with environmental research and assessment of risk to ecosystems and human health from environmental hazardous.

Owing to the fact that Equations (1) and (2) are innovative tools for data-processing of measurable variables, but as aforementioned there are already established Directives and ISO requirements using classical methods for data-processing of measurands from MS experiments, imperative questions arise:

(i) How can the new formulas belong constructively to classical methods for the analytical practice; and

(ii) and which are their advantages, comparing with known theoretical methods for mass spectrometric based analysis of chemical compounds?

In the light of these questions, if one considers, first the concept of the new method relatively closely, then one could immediately draw distinction between the novel approaches to data- processing of MS measurands comparing with known methods.

Thus, in addressing questions (i) and (ii), I shall sketch complexity of the models.

To begin with, Equations (1), (2), and (4) can be regarded as novelty to the analytical mass spectrometry as methodological development of the field [30], rather than as an explicitly elaborated tool for purposes of polymer research.

Since, polymeromics belongs to omics-methods for analysis, the new Equations (1), (2), and (4) could find prospective application to determine polymers, as well.

However, the overall complexity of studying polymers already highlighted in preceding sections of this study should be taken into account.

Moreover, the validity of the discussed formulas is tested on few examples of polymers; furthermore, containing relatively simple chemical compositions [59].

Advantages of the equations, that are, particularly prominent are associated with in ongoing debates emerging from method performances of conventional MS methods for data-processing of measurable variables of both low- and high-molecular weight analytes in complex environmental and food samples as well as biological fluids [30,49,53] as well as applicability of the methods for mass spectrometry to obtain exact analyte 3D molecular structure in such samples.

Due to these reasons, herein, I would like to introduce methodology used to

write Equations (1), (2), and (4) which distinguished sharply from available methods for both quantitative and structural analysis based on mass spectrometry. The so-called mass spectrometric measurands, i.e., mass-to-charge and intensity values of parent and products ions of in fact isotopomers of any analyte are described as random variables.

In the light of the latter statement, however, the reader is referred to consider the IUPAC definition of isotopomer [114], and mass spectrometric molecular isotopologies as shown in works [30,49,53], because of within the framework of a MS experiment there is obtained exact data on isotope composition of the atoms in the analyte molecule.

However, m/z measurands can be obtained experimentally via calibration using data on MS ions of known m/z quantity [115] owing to the fact that calibrates should be chosen with regard to both the design of the MS instrument and application purposes. In addition, there should be accounted for simple sample preparation of the standards, abundance and stable signals, as well as a lack of memory effect. Often, it can be hard even not possible to cover the sketched requirement without compromises, regarding the analytical information.

Therefore, in studying complex samples of unknown analytes even LMWs ones, due to lack of suitable standard or standard requirements there could be unable to obtain reliable analytical information via the already established protocols.

Moreover, the standard protocols based on knowledge of natural isotopic distributions of elements applied to determine quantitatively and to elucidate structurally unknown compounds in mixtures by interpreting their mass spectra, particularly, highlighting polymers could be altered, as well. In cases of oligomers and polymers when there are heady atoms of chalogenides, then the characteristic isotopic signatures of the MS patterns can be deduced by inspection and can be relatively reliably determined [116]. In cases of analytes having a lack of atoms showing characteristic isotopic signatures, then the upper limit on the number of C-atom can be obtained examining the abundance of all-^{12}C-versions of the analyte ion to that of corresponding ^{13}C-isotopic form, but large molecules show Gaussian distributions of C-isotopes centred on the average molecular weight and having unusual carbon isotopic abundance. Thus, the ratio of intensity data on experimental MS peaks of isotopomers $^{13}C/^{12}C$ are lower than theoretically predicted and expected ones via standard methods.

Furthermore, there is fluctuation in elemental composition, due to isotope fractionation obtained by (bio)chemical and geochemical processes, which perturb the value of the isotope ratio among isotopomers of the same atom; thus, yielding to errors in omics-methods [117]. Omics methods do not account for fluctuations of measurands.

Due to reasons sketched above accurately determining of analyte quantity or molecular structure among a set of candidate structures, particularly, highlighting complex multicomponent mixtures of unknown analytes still represents a challenging analytical task. The latter challenges are associated with both the MS measurands even using ultra-high accuracy analytical instrumentation showing excellent features and already routinely implemented standard methods for data-processing of MS measurable variables.

Having secured the latter standpoint, we could then say that exact quantitative and structural determination of analytes mass spectrometrically can be achieved mostly via complementary employment of different experimental and theoretical methods and techniques.

Owing to fluctuations of the experimental measurable data on both low and high molecular weight analytes we can say that theoretically, a mass spectrum of any analyte can only be reliably described and predicted via exact approaches allowing generation of random numbers, because of they allow us to account for the fluctuations of MS measurands. The alternative known methods, however, do not succeed in talking the latter issue.

Conversely, the stochastic dynamics model Equations (1), (2), and (4) are designed in order to solve the latter problem.

Model Equation (1) is based on modified formula of the Box–Müller method for generating such random numbers. Concentrate on its basic Equation (C1) [118]. The shown, then, Equation (C2) is derived from the former one. The x and $\langle x \rangle$ denote stochastic variable and its average value, while P_1 and P_2 are random numbers. The σ^2 denotes variance, which is given by Equation (C3) [119,120]. If intensity measurand of any analyte peak is described as random variable then there can be written $x = I$. Studying a series of low molecular weight organics, metal-organics and inorganics it has been proven that $\ln P_1 = -17.0533_{(7)}$ is a constant for all MS measurable variable intensity (I) of any MS peaks over any span of scan time under a broad spectrum of ionisation methods and techniques used to measure mass spectrum of any analyte such as, for example ESI-, APSI-, matrix-assisted laser/desorption/ionisation mass spectrometry, collision induced dissociation tandem operation mode, and more [30,47,48–59,119,120]. On this base, further, we write Equation (C4). In the latter context, there has been proposed a functional relation $A = -2\sigma^{2'}$. $\ln P_1$ having not only statistical significance, but rather physical meaning. The variance parameters σ^2 and $\sigma^{2'}$ are independent of each other. Within the framework of Ornstein-Uhlenbeck's approximation ($\sigma^{2'} = 2\beta^2 D$) to σ^2 and Einstein's approximation to parameter $\beta = 3 \times 10^{-8}$ [119] Equation (C4) is given by equation (C5). The substitution of the mentioned above relations yields to Equation (1). It is exact quantitative model connecting between diffusion parameter and experimental MS intensity written as $(I - \langle I \rangle)^2$. The parameter '$A$' is obtained via SineSqr curve fitting of experimental relation $(I - \langle I \rangle)^2 = f(t)$ where t denote time. Therefore, the stochastic dynamics methods are already proven as universally applicable approach to low-molecular weight organics, inorganics, metal-organics within the framework of series of ionisation mass spectrometric methods and techniques.

Parameter 'A' accounts for temporal distribution of measurable variable intensity (I) of MS peak of analyte product and parent ion over any random span of scan time of measurements.

Depending on complexity of function $(I - \langle I \rangle)^2 = f(t)$ or the temporal behavior of measurand intensity over a studied span of scan time, there can be expected deviations from absolute correlation ($|r| = 1$) of SineSqr curve fitting procedure [53,119]. In solving the latter problem, Equation (1) there is simplified, using approximation that $A \equiv 2\langle (I - \langle I \rangle)^2 \rangle$; thus, writing Equation (2). It is capable of

exact quantifying analytes and determining 3D molecular structure of analyte on the base on MS soft-ionization methods [54].

At this point it would be easy to see the major advantages of Equation (2) comparing with the classical tools for data processing of measurable variables of MS experiments: (a) It is exact model, yielding to $|r| = 1$ quantifying analytes in complex samples, including biological fluids [53,54,120]; (b) it is applicable in parallel for exact determining of analyte 3D molecular and electronic structures accounting for subtle electronic effects such as tautomers, in addition to protomers, and isotopomers [49,52]; (c) it is applicable to any type of chemical compounds as aforementioned encompassing, organics, inorganics, metal-organics, and organometallics; (d) and within the framework of a set available ionization MS methods and techniques [30,47,48–59,119,120].

Furthermore, the stochastic dynamics approach has been validated empirically via independent instrumental method for analysis such as chromatography [121]; thus, sowing $|r| = 0.99998$. The latter study includes analysis of mixtures of steroids using a set of mathematical and statistical methods for data-processing of chromatographic patterns.

Conversely, analyses reported, so far, this study persuasively illustrates the great capability of the discussed stochastic dynamics model equations to determine significantly more complex analytes from perspective of molecular structure such as polymers; furthermore, in multicomponent commercial sample of composite biodegradable materials containing 20,416 (Cell_5) and 17,495 (Cell_7) detected features.

The bulk in concepts used to experimentally design MS analysis of everyday bio-based or biodegradable, or both of these bags for foodstuffs as comprehensively described in works [13,16] are based on in vitro bioassays of, in total, detected up to 41,395 chemicals per individual sample. There is shown that ca. 67% of studied samples induced baseline toxicity. Circa 42% of them induce oxidative stress and at about 23% exhibit antiandrogenicity. One sample of plastics shows estrogenicity. Thus, there has been highlighted the potential risk for the environmental safety and human health.

However, I would like to discuss in this section why we may expect to find toxicity of even analysing biodegradable plastics from perspective of detailed MS analysis of composite materials reported, first in this study. **Figures 2** and **8** reveal a complex mixture of not only biodegradable polymers and their oligomer associates, but also synthetic additives and a large number of oxidised and chemically reacted polymers and oligomeric associates.

Therefore, my claim is that there is not surprise that individual samples of commercial packing materials of even highlighted as biodegradable and renewable composite materials could possess toxicological effect to a certain degree. The validity of conclusions strongly depends on a large number of specific and often unknown or commercially not highlighted components of packing polymer composite materials. This fact, requires an in-depth chromatographic and MS determining as well as structural analysis of polymers and oligomers in addition to their products of degradation; if any.

Also, there is requested analysis of additives and other components in order to

detail on functional relation between type of composite of commercial packing even biodegradable one and its potential toxicological effect on environment and human health.

If we opt for verification of claim about any potential toxicological effect in order to make it rigour and certain, then, it should be validated outside including results not only to very special commercially available composite polymers, but also to laboratory polymer compositions of standard components examined under special environmentally mimicked experimental conditions in order to justify a claim that there could be toxicological effect to human from even biodegradable plastics used commercially at an industrial scale.

In what follows in this section, I would like to attempt to make headway on advantages of the complementary application of the innovative stochastic dynamics MS method and vibration spectroscopy, particularly underlying in this study infrared spectroscopy for determining polymers, despite the fact that vibration spectroscopy is routinely used to the environmental research [5,7–12].

As we already have seen in preceding sections interpreting mass spectra of multicomponent composite polymers containing in the case of this study within 20,416–17,495 chemicals per sample is not so easy. We must not escape a notice that vibration spectroscopy provides very fast, cheap, and again direct analysis of polymers.

Furthermore, the methods are not only already implemented into the analytical practice, but also provide not only databases of FTIR-spectra of standard polymers; for instance [62], but also there are atlas of both IR and Ramans spectra of LMWs used to additives.

Despite, vibration spectroscopic methods are restricted to study macrocomponents in mixtures. Furthermore, both quantitative and structural analyses of individual analytes via direct analysis can be achieved studying relatively simple mixtures of analytes [48].

Thus, vibration spectroscopy allows us to treat both quantitatively and structurally commercial composites of (bio)polymers. Perhaps, it might be possible to claim of reliable analytical information, but mainly in cases when there are relatively low numbers and macro components of the polymer mixtures of food packing. An alternative standpoint; if any, then might be problematic and even speculative claim of erroneous analysis, despite, the advantages of the vibration spectroscopic methods sketched, above.

Conversely, the employment of ultra-high accuracy methods of mass spectrometry and innovative Equation (2) for data processing of MS measurands there is achieved exact direct analysis of individual analytes; furthermore, polymers in complex mixtures of food packing of biopolymers containing as aforementioned up to 20,416 chemicals per sample. Nevertheless, depending on complexity of polymer molecular structure difficulties could remain for its exact 3D determination, mass spectrometrically. The latter problem can be traced, respectively, solved via systematic further research effort on applying Equations (2)–(4) to determine quantitative and structurally (bio)polymer composite materials.

5. Conclusion

What could we conclude, considering the presented results from the preceding subsections of the paper? The answer to the latter question can be generated mainly by the results from subsection 3.4 dealing with correlative analysis between theory and experiment, because of the chemomeric assessment of the degree of linear correlation between theoretical and experimental mass spectrometric data justifies empirically the validity and significant applicability of the innovative stochastic dynamics model Equation (2) and its derivative Equation (4) to describe, assign, and predict mass spectra reliably even examining complex mixtures of composite polymers used to biodegradable food packing materials: furthermore, at an industrial scale. Since, Equations (2) and (4) are designed to tell us what is the quantity of the analyte in mixture, which analyte occurs in the mixture, and which are it 3D molecular and electronic structures the achieved excellent-to-exact parameter $|r| = 0.99981$ examining species of PPG in everyday bio-based or biodegradable, bags for foodstuffs indicates not only the great prospective and applicability of the discussed formulas to develop the structural mass spectrometry, but also their potential application at an industrial scale since the object of analysis are commercially distributed packing for foods of biodegradable polymers. Since, the study is designed to assess what contribution Equations (2) and (4) could have to purposes of environmental chemistry and mass spectrometric based determining of environmental pollution of plastics, the obtained remarkably high chemometric parameters clearly indicates that the two formulas appear prospective tool for mass spectrometric based monitoring and analysis of both synthetic and biodegradable plastics in real samples from the environment, because of as highlighted through the paper the object of analysis represent highly complex trade composite polymer materials. As can be seen there is achieved reliable, highly justifiable and verifiable by independent both experimental and theoretical methods content of polymers in composite materials. Owing to the fact that the model Equations (2) and (4) have been tested so far on a scarce number of polymers looking at a laboratory synthetic polymer mixture in work [59] and commercial composite complex polymer reported, herein, further research effort aims to establish a tendency claim, regarding, the potential industrial scale application of the innovative model formulas to determine complex composites of biodegradable and renewable polymer materials.

Funding: The author thanks the Deutsche Forschungsgemeinschaft (Funder ID: http://dx. doi.org/10. 13039/50110 00016 59; grant 255/22–1); Alexander von Humboldt Stiftung; Deutscher Akademischer Austausch Dienst for grant within priority program Stability Pact South-Eastern Europe.

Supporting information: Mass spectrometric, chromatographic data theoretical data (Appendixes A–C).

Data availability: Experimental mass spectrometric infrared spectroscopic raw-data are publicly available and can be downloaded free of charge [60].

Conflict of interest: The author declares no conflict of interest.

Abbreviations

ANOVA	Analysis of variance (chemometric method)
APCI	Atmospheric pressure chemical ionization (mass spectrometric method)
BOMD	Born–Oppenheimer molecular dynamics
CB	Carbohydrate
LMW	Low-molecular-weight (analytes)
DFT	Density functional theory (quantum chemical method)
DoF	Number of points—number of parameters
D_{QC}	Quantum chemical diffusion parameter according to Arrhenius's theory
D_{SD}, D_{SD}''	Stochastic dynamic diffusion parameters according to our theory
ESI	Electrospray ionization (mass spectrometric method)
GS	Ground state
Glc	Glucose
HPLC	High performance liquid chromatography
I	Intensity of mass spectrometric peak (variable)
ISOP	Polyisoprene
m/z	Mass-to-charge (mass spectrometric variable)
MD	Molecular dynamics
MM	Molecular mechanics
MS	Mass spectrometry
MS/MS	Tandem mass spectrometric operation mode
PCM	Polarizable continuum method
PES	Potential energy surface
PEG	Poly(ethylenglycol)
PEGME	Poly(ethylenglycol)methylether
PEGDME	Polyethylene glycol dimethyl ether
PEO	Poly(ethylene oxide)
PPO	Poly(propylene oxide)
PLA	Polylactide
PPG	Poly(propylene glycol)
|r|	Statistical coefficient of linear correlation (chemometrics)
RT	Retention time
sd(yEr±)	Standard deviation (chemometrics)
se(yEr±)	Standard error (chemometrics)
TIA	Trapezoidal integration approach
TS	Transition state
ΔG	(Difference) in free Gibbs energy

References

1. Zhang H, Su Z, Wang X. Starch-Based Rehealable and Degradable Bioplastic Enabled by Dynamic Imine Chemistry. ACS Sustainable Chemistry & Engineering. 2022; 10(26): 8650-8657. doi: 10.1021/acssuschemeng.2c02537
2. Shafqat A, Al-Zaqri N, Tahir A, et al. Synthesis and characterization of starch based bioplatics using varying plant-based ingredients, plasticizers and natural fillers. Saudi Journal of Biological Sciences. 2021; 28(3): 1739-1749. doi:

10.1016/j.sjbs.2020.12.015
3. Rizzarelli P, Leanza M, Rapisarda M. Investigations into the characterization, degradation, and applications of biodegradable polymers by mass spectrometry. Mass Spectrometry Reviews. Published online November 28, 2023. doi: 10.1002/mas.21869
4. Chia HN, Wu BM. Recent advances in 3D printing of biomaterials. Journal of Biological Engineering. 2015; 9(1). doi: 10.1186/s13036-015-0001-4
5. Abed SH, Shamkhi AF, Heydaryan K, et al. Sol-gel Pechini preparation of CuEr2TiO6 nanoparticles as highly efficient photocatalyst for visible light degradation of acid red 88. Ceramics International. 2024; 50(13): 24096-24102. doi: 10.1016/j.ceramint.2024.04.141
6. Chen X, Yan S, Wang H, et al. Aerobic oxidation of starch catalyzed by isopolyoxovanadate Na4Co(H2O)6V10O28. Carbohydrate Polymers. 2015; 117: 673-680. doi: 10.1016/j.carbpol.2014.10.066
7. Kiani Z, Mirjalili S, Heydaryan K, et al. Harmonizing nature and nanotechnology: Phytoextract-mediated synthesis of Ag-doped ZnO nanoparticles using Lavandula stoechas extract for environmental and biomedical applications. Journal of Drug Delivery Science and Technology. 2024; 96: 105708. doi: 10.1016/j.jddst.2024.105708
8. Khanjari Z, Chamani E, Heydaryan K, et al. Unlocking the therapeutic potential: Green synthesized zinc oxide/silver nanoparticles from Sophora pachycarpa for anticancer activity, gene expression analysis, and antibacterial applications. Materials Today Communications. 2024; 39: 109214. doi: 10.1016/j.mtcomm.2024.109214
9. Ghazi RA, Jasim AS, Heydaryan K, et al. Biosynthesis of Ag-Doped CuO Nanoparticles Using Heracleum persicum Extract for Enhanced Antibacterial and Photocatalytic Dye Degradation Properties. Plasmonics. 2024. doi: 10.1007/s11468-024-02298-1
10. Kashi MA, Heydaryan K, Khojasteh H, et al. Green Synthesis of Ag NPs/rGO Nanocomposite for Use as a Non-enzymatic Sensor of H2O2. Plasmonics. 2024. doi: 10.1007/s11468-024-02330-4
11. Khojasteh H, Heydaryan K, Aspoukeh P, et al. Characterization and Application of CuO Nanoparticles in Gelatin-Glycerol Coatings for Enhanced Shelf Life of Strawberries. Plasmonics. 2024. doi: 10.1007/s11468-024-02345-x
12. Abed SH, Madhi RA, Heydaryan K, et al.Shamkhi A. Green synthesis of gold-doped ZnFe2O4 nanoparticles using Crataegus monogyna leaf extract: characterization, antibacterial, and efficient degradation of methylene blue and eriochrome black T pollutants. Biomass Conversion and Biorefinery. 2024. doi: 10.1007/s13399-024-05337-3
13. Zimmermann L, Dombrowski A, Völker C, et al. Are bioplastics and plant-based materials safer than conventional plastics? In vitro toxicity and chemical composition. Environment International. 2020; 145: 106066. doi: 10.1016/j.envint.2020.106066
14. Binda G, Costa M, Supraha L, et al. Untangling the role of biotic and abiotic ageing of various environmental plastics toward the sorption of metals. Science of The Total Environment. 2023; 893: 164807. doi: 10.1016/j.scitotenv.2023.164807
15. Anna V, Rimma S, Lev O, et al. GC determination of N-nitrosamines by supersonic molecular beam MS equipped with triple quadrupole analyzer, GC/SMB/QQQ/MS. Analytica Chimica Acta. 2011; 685(2): 162-169. doi: 10.1016/j.aca.2010.11.026
16. Zimmermann L, Dierkes G, Ternes TA, et al. Benchmarking the in Vitro Toxicity and Chemical Composition of Plastic Consumer Products. Environmental Science & Technology. 2019; 53(19): 11467-11477. doi: 10.1021/acs.est.9b02293
17. Regulation (EC) No 1935/2004 of the European Parliament and the Council. On materials and articles intended to come into contact with food and repealing Directives 80/590/EEC and 89/109/EEC. Official Journal of the European Union L338/4. 2004.
18. European Commission. European Commission (2011) Commission regulation (EU) No 10/2011 of 14 January 2011 on plastic materials and articles intended to come into contact with food. Official Journal of the European Union L12/1. 2011.
19. Bos TS, Pirok BWJ, Karlson L, et al. Fingerprinting of hydroxy propyl methyl cellulose by comprehensive two-dimensional liquid chromatography-mass spectrometry of monomers resulting from acid hydrolysis. Journal of Chromatography A. 2024; 1722: 464874. doi: 10.1016/j.chroma.2024.464874
20. Kumar A, Dutta D, Kalita D, et al. Extraction, physicochemical and structural characterisation of palm grass leaf fibres for sustainable and cleaner production of textile and allied cellulosic applications. Journal of Cleaner Production. 2024; 448: 141733. doi: 10.1016/j.jclepro.2024.141733
21. Xue P, Liu M, Yang H, et al. Mechanism study on pyrolysis interaction between cellulose, hemicellulose, and lignin based on photoionization time-of-flight mass spectrometer (PI-TOF-MS) analysis. Fuel. 2023; 338: 127276. doi:

10.1016/j.fuel.2022.127276
22. Chen D, Cen K, Zhuang X, et al. Insight into biomass pyrolysis mechanism based on cellulose, hemicellulose, and lignin: Evolution of volatiles and kinetics, elucidation of reaction pathways, and characterization of gas, biochar and bio-oil. Combustion and Flame. 2022; 242: 112142. doi: 10.1016/j.combustflame.2022.112142
23. Zhang D, Loomer M, Gamez G. Quantitative analysis of biopolymers in lignocellulosic biomass feedstocks via laser-assisted micro-pyrolysis flowing atmospheric-pressure afterglow high-resolution ambient mass spectrometry. Talanta. 2024; 268: 125333. doi: 10.1016/j.talanta.2023.125333
24. Ruggero F, Carretti E, Gori R, et al. Monitoring of degradation of starch-based biopolymer film under different composting conditions, using TGA, FTIR and SEM analysis. Chemosphere. 2020; 246: 125770. doi: 10.1016/j.chemosphere.2019.125770
25. Tolonen LK, Juvonen M, Niemelä K, et al. Supercritical water treatment for cello-oligosaccharide production from microcrystalline cellulose. Carbohydrate Research. 2015; 401: 16-23. doi: 10.1016/j.carres.2014.10.012
26. Osorio J, Aznar M, Nerín C, et al. Comparison of LC-ESI, DART, and ASAP for the analysis of oligomers migration from biopolymer food packaging materials in food (simulants). Analytical and Bioanalytical Chemistry. 2021; 414(3): 1335-1345. doi: 10.1007/s00216-021-03755-0
27. Golon A, González FJ, Dávalos JZ, et al. Investigating the Thermal Decomposition of Starch and Cellulose in Model Systems and Toasted Bread Using Domino Tandem Mass Spectrometry. Journal of Agricultural and Food Chemistry. 2013; 61(3): 674-684. doi: 10.1021/jf302135k
28. Ghiulai R, Galusca M, Sisu I, et al. High resolution mass spectrometric characterization of amino linked oligosaccharides—a preliminary study. Open Chemistry. 2013; 11(8): 1309-1319. doi: 10.2478/s11532-013-0265-9
29. Jiang J, Wang X. Adsorption of Hg(II) ions from aqueous solution by thiosemicarbazide-modified cellulose adsorbent. BioResources. 2019; 14(2): 4670-4695. doi: 10.15376/biores.14.2.4670-4695
30. Ivanova B. Special Issue with Research Topics on "Recent Analysis and Applications of Mass Spectra on Biochemistry." International Journal of Molecular Sciences. 2024; 25(4): 1995. doi: 10.3390/ijms25041995
31. Wang Z, Liu PK, Li L. A Tutorial Review of Labeling Methods in Mass Spectrometry-Based Quantitative Proteomics. ACS Measurement Science Au. 2024. doi: 10.1021/acsmeasuresciau.4c00007
32. Calvano CD, Cataldi TRI, Kögel JF, et al. Structural Characterization of Neutral Saccharides by Negative Ion MALDI Mass Spectrometry Using a Superbasic Proton Sponge as Deprotonating Matrix. Journal of the American Society for Mass Spectrometry. 2017; 28(8): 1666-1675. doi: 10.1007/s13361-017-1679-y
33. Wesdemiotis C. Multidimensional Mass Spectrometry of Synthetic Polymers and Advanced Materials. Angewandte Chemie International Edition. 2017; 56(6): 1452-1464. doi: 10.1002/anie.201607003
34. Wesdemiotis C, Williams-Pavlantos KN, Keating AR, et al. Mass spectrometry of polymers: A tutorial review. Mass Spectrometry Reviews. 2023; 43(3): 427-476. doi: 10.1002/mas.21844
35. Lattimer R. Tandem mass-spectrometry of poly(ethylene glycol) proton-attachment and deuteron-attachment ions. International Journal of Mass Spectrometry. 1992; 116: 23-36. doi: 10.1016/0168-1176(92)80017-U
36. Li X, Guo L, Casiano-Maldonado M, et al. Top-Down Multidimensional Mass Spectrometry Methods for Synthetic Polymer Analysis. Macromolecules. 2011; 44(12): 4555-4564. doi: 10.1021/ma200542p
37. Buck-Wiese H, Fanuel M, Liebeke M, et al. Discrimination of β-1,4- and β-1,3-Linkages in Native Oligosaccharides via Charge Transfer Dissociation Mass Spectrometry. Journal of the American Society for Mass Spectrometry. 2020; 31(6): 1249-1259. doi: 10.1021/jasms.0c00087
38. Wesdemiotis C, Solak N, Polce MJ, et al. Fragmentation pathways of polymer ions. Mass Spectrometry Reviews. 2011; 30(4): 523-559. doi: 10.1002/mas.20282
39. Stephens CH, Shrestha B, Morris HR, et al. Minimally invasive monitoring of cellulose degradation by desorption electrospray ionization and laser ablation electrospray ionization mass spectrometry. The Analyst. 2010; 135(9): 2434. doi: 10.1039/c0an00155d
40. Pfenninger A, Karas M, Finke B, Stahl B. Structural analysis of underivatized neutral human milk oligosaccharides in the negative ion mode by nano-electrospray MSn (Part 2). Journal of the American Society for Mass Spectrometry. 2002; 13: 1341-1348. doi: 10.1016/S1044-0305(02)00646-3
41. Montaudo G, Samperi F, Montaudo MS. Characterization of synthetic polymers by MALDI-MS. Progress in Polymer Science. 2006; 31(3): 277-357. doi: 10.1016/j.progpolymsci.2005.12.001

42. Schulz H, Baranska M. Identification and quantification of valuable plant substances by IR and Raman spectroscopy. Vibrational Spectroscopy. 2007; 43(1): 13-25. doi: 10.1016/j.vibspec.2006.06.001
43. Alves APP, de Oliveira LPZ, Castro AAN, et al. The structure of different cellulosic fibres characterized by Raman spectroscopy. Vibrational Spectroscopy. 2016; 86: 324-330. doi: 10.1016/j.vibspec.2016.08.007
44. Tallarico S, Bonacci S, Mancuso S, et al. Quali-quantitative monitoring of chemocatalytic cellulose conversion into lactic acid by FT-NIR spectroscopy. Spectrochimica Acta Part A: Molecular and Biomolecular Spectroscopy. 2021; 250: 119367. doi: 10.1016/j.saa.2020.119367
45. Kotatha D, Rungrodnimitchai S. Synthesis and Characterization of Nanofiber of Oxidized Cellulose from Nata De Coco. International Journal of Chemical Engineering. 2018; 2018: 1-12. doi: 10.1155/2018/2787035
46. Document 31996L0023: Commision Decision of 12.08.2002 implementing Council Directive 96/23/EC concerning the performance of analytical methods and the interpretation of results; notified under document number C(2002) 3044; Text with EEA relevance 2002/657/EC. Official Journal of the European Union L 221/8. 2022.
47. Ivanova B, Spiteller M. Electrospray ionization stochastic dynamic mass spectrometric 3D structural analysis of ZnII-ion containing complexes in solution. Inorganic and Nano-Metal Chemistry. 2021; 52(12): 1407-1429. doi: 10.1080/24701556.2021.1956963
48. Ivanova B, Tsalev D, Arnaudov M. Validation of reducing-difference procedure for the interpretation of non-polarized infrared spectra of n-component solid mixtures. Talanta. 2006; 69(4): 822-828. doi: 10.1016/j.talanta.2005.11.026
49. Ivanova B. Stochastic Dynamic Mass Spectrometric Quantitative and Structural Analyses of Pharmaceutics and Biocides in Biota and Sewage Sludge. International Journal of Molecular Sciences. 2023; 24(7): 6306. doi: 10.3390/ijms24076306
50. Ivanova B, Spiteller M. Stochastic dynamic mass spectrometric quantification of steroids in mixture—Part II. Steroids. 2020; 164: 108750. doi: 10.1016/j.steroids.2020.108750
51. Ivanova B, Spiteller M. Stochastic Dynamic Mass Spectrometric Approach to Quantify Reserpine in Solution. Analytical Chemistry Letters. 2020; 10(6): 703-721. doi: 10.1080/22297928.2020.1865834
52. Ivanova B, Spiteller M. Chapter 1: Mass spectrometric and quantum chemical treatments of molecular and ionic interactions of a flavonoid-O-glycoside—A stochastic dynamic approach. In: Advances in Chemistry Research. NOVA Science Publishers, New York; 2022. pp. 1-126.
53. Ivanova B, Spiteller M. Stochastic Dynamic Electrospray Ionization Mass Spectrometric Quantitative Analysis of Metronidazole in Human Urine. Analytical Chemistry Letters. 2022; 12(3): 322-348. doi: 10.1080/22297928.2022.2086822
54. Ivanova B, Spiteller M. Exact Quantifying of Mass Spectrometric Variable Intensity of Analyte Peaks with Respect to Experimental Conditions of Measurements—A Stochastic Dynamic Approach. Analytical Chemistry Letters. 2022; 12(5): 542-561. doi: 10.1080/22297928.2022.2142844
55. Ivanova B, Spiteller M. Stochastic dynamic ultraviolet photofragmentation and high collision energy dissociation mass spectrometric kinetics of triadimenol and sucralose. Environmental Science and Pollution Research. 2022; 30(12): 32348-32370. doi: 10.1007/s11356-022-24259-z
56. Ivanova B, Spiteller M. Stochastic dynamic quantitative and 3D structural matrix assisted laser desorption/ionization mass spectrometric analyses of mixture of nucleosides. Journal of Molecular Structure. 2022; 1260: 132701. doi: 10.1016/j.molstruc.2022.132701
57. Ivanova B. 3D structural analysis of alanyl-containing peptides of silac-proteomics—an approach to stochastic dynamics. SSNR eJournal. 2023. doi: 10.2139/ssrn.4498960
58. Upadyshev M, Ivanova B, Motyleva S. Mass Spectrometric Identification of Metabolites after Magnetic-Pulse Treatment of Infected Pyrus communis L. Microplants. International Journal of Molecular Sciences. 2023; 24(23): 16776. doi: 10.3390/ijms242316776
59. Ivanova B. Stochastic dynamics mass spectrometric structural analysis of poly(methyl methacrylate). Universal Journal of Carbon Research. 2024: 60-88. doi: 10.37256/ujcr.2120244425
60. Zimmermann L, Zimmermann L, Dombrowski A, et al. Raw data for “Are bioplastics and plant-based materials safer than conventional plastics? In vitro toxicity and chemical composition”. Available online: https://zenodo.org/records/4004763 (accessed on 27 August 2020).
61. Centexbel. Gudelines for data-analysis, calibration, and prediction. SAFIR project WP3/SMT4-CT96-2136. VTT Rakennus; 2002.
62. Villegas-Camacho O, Alejo-Eleuterio R, Francisco-Valencia I, et al. FTIR-Plastics: A Fourier Transform Infrared

Spectroscopy dataset for the six most prevalent industrial plastic polymers. Data in Brief. 2024; 55: 110612. doi: 10.1016/j.dib.2024.110612
63. Frisch M, Trucks G, Schlegel H, et al. Gaussian 09, 98. Gaussian, Inc., Pittsburgh, Wallingford CT; 2009.
64. Aidas K, Angeli C, Bak K et al. The Dalton quantum chemistry program system. Wiley Interdisciplinary Reviews: Computational Molecular Science. 2014; 4: 269-284. doi: 10.1002/wcms.1172
65. Gordon MS, Schmidt MW. Advances in electronic structure theory. Theory and Applications of Computational Chemistry. 2005; 1167-1189. doi: 10.1016/b978-044451719-7/50084-6
66. Nielsen A, Holder A. Gauss View 5.0, User's Reference. Pittsburgh GausView03 Program Package. GAUSSIAN Inc.; 2009.
67. Burkert U, Allinger N. Molecular mechanics in ACS Monograph 177. American Chemical Society, Washington D.C.; 1982.
68. Allinger NL. Conformational analysis. 130. MM2. A hydrocarbon force field utilizing V1 and V2 torsional terms. Journal of the American Chemical Society. 1977; 99(25): 8127-8134. doi: 10.1021/ja00467a001
69. Kelley C. Iterative Methods for optimization. SIAM Front. Appl. Mathematics. 2009; 18.
70. Otto M. Chemometrics, 3rd ed. Wiley, Weinheim; 2017.
71. Apache OpenOffice. Available online: http://de.openoffice.org (accessed on 3 May 2024).
72. Madsen K, Nielsen H, Tingleff T. Informatics and mathematical modelling, 2nd ed. DTU Press; 2004.
73. Miller J, Miller J. Statistics and chemometrics for analytical chemistry. Pentice Hall, London; 1988.
74. Taylor J. Quality assurance of chemical measurements. Lewis Publishers, Inc.; 1987.
75. Schroee G, Trenkler D. Exact and randomization distributions of Kolmogorov-Smirnov tests two or three samples. Computational Statistics & Data Analysis. 1995; 20: 185-202. doi: 10.1016/0167-9473(94)00040-P
76. Fay MP, Proschan MA. Wilcoxon-Mann-Whitney or t-test? On assumptions for hypothesis tests and multiple interpretations of decision rules. Statistics Surveys. 2010; 4. doi: 10.1214/09-ss051
77. Freidlin B, Gastwirth JL. Should the Median Test be Retired from General Use? The American Statistician. 2000; 54(3): 161-164. doi: 10.1080/00031305.2000.10474539
78. Kunov-Kruse AJ, Riisager A, Saravanamurugan S, et al. Revisiting the Brønsted acid catalysed hydrolysis kinetics of polymeric carbohydrates in ionic liquids by in situ ATR-FTIR spectroscopy. Green Chemistry. 2013; 15(10): 2843. doi: 10.1039/c3gc41174e
79. Jackson A, Yates H, Scrivens J, et al. The application of matrix-assisted laser desorption/ionization combined with collision-induced dissociation to the analysis of synthetic polymers. Rapid Communications Mass Spectrometry. 1996; 10: 1668-1674. doi: 10.1002/(SICI)1097-0231(199610)10:13<1668::AID-RCM703>3.0.CO;2-I
80. Scrivens J, Jackson A, Yates H, et al. The effect of the variation of cation in the matrix-assisted laser desorption/ionisation collision induced dissociation (MALDI-CID) spectra of oligomeric systems. International Journal of Mass Spectrometry. 1997; 165: 363-375. doi: 10.1016/S0168-1176(97)00239-5
81. Jackson AT, Green MR, Bateman RH. Generation of end-group information from polyethers by matrix-assisted laser desorption/ionisation collision-induced dissociation mass spectrometry. Rapid Communications in Mass Spectrometry. 2006; 20(23): 3542-3550. doi: 10.1002/rcm.2773
82. Lattimer R. Tandem mass-spectrometry of lithium-attachment ions from polyglycols. Journal of the American Society for Mass Spectrometry. 1992; 3: 225-234. doi: 10.1016/1044-0305(92)87006-K
83. Lattimer R. Tandem mass-spectrometry of poly(ethylene glycol) lithium-attachment ions. Journal of the American Society for Mass Spectrometry. 1994; 5: 1072-1080. doi: 10.1016/1044-0305(94)85068-2
84. Selby T, Wesdemiotis C, Lattimer R. Dissociation characteristics of [M-X]-ions (X = H, Li, K) from linear and cyclic polyglycols. Journal of the American Society for Mass Spectrometry. 1994; 5: 1081-1092. doi: 10.1016/1044-0305(94)85069-0
85. Lattimer R. Mass spectral analysis of low-temperature pyrolysis products from poly(ethylene glycol). Journal of Analytical and Applied Pyrolysis. 2000; 56: 61-78. doi: 10.1016/S0165-2370(00)00074-7
86. Scionti V, Katzenmeyer BC, Erdem NS, et al. Interfacing Multistage Mass Spectrometry with Liquid Chromatography or Ion Mobility Separation for Synthetic Polymer Analysis. European Journal of Mass Spectrometry. 2012; 18(2): 113-137. doi: 10.1255/ejms.1175
87. D'Alexandri FL, Gozzo FC, Eberlin MN, et al. Electrospray ionization mass spectrometry analysis of polyisoprenoid alcohols via Li+ cationization. Analytical Biochemistry. 2006; 355(2): 189-200. doi: 10.1016/j.ab.2006.06.014
88. Snyder SR, Wesdemiotis C. Elucidation of Low Molecular Weight Polymers in Vehicular Engine Deposits by

Multidimensional Mass Spectrometry. Energy & Fuels. 2020; 35(2): 1691-1700. doi: 10.1021/acs.energyfuels.0c02702
89. Voorhees K, Baugh S, Stevenson D. An investigation of the thermal degradation of poly(ethylene glycol). Journal of Analytical and Applied Pyrolysis. 1994; 30: 47-57. doi: 10.1016/0165-2370(94)00803-5
90. Endres KJ, Dilla RA, Becker ML, et al. Poly(ethylene glycol) Hydrogel Crosslinking Chemistries Identified via Atmospheric Solids Analysis Probe Mass Spectrometry. Macromolecules. 2021; 54(17): 7754-7764. doi: 10.1021/acs.macromol.1c00765
91. Chen H, He M, Pei J, et al. Quantitative Analysis of Synthetic Polymers Using Matrix-Assisted Laser Desorption/Ionization Time-of-Flight Mass Spectrometry. Analytical Chemistry. 2003; 75(23): 6531-6535. doi: 10.1021/ac0344034
92. Okuno S, Wada Y, Arakawa R. Quantitative analysis of polypropyleneglycol mixtures by desorption/ionization on porous silicon mass spectrometry. International Journal of Mass Spectrometry. 2005; 241(1): 43-48. doi: 10.1016/j.ijms.2004.10.022
93. Boulos S, Nyström L. UPLC-MS/MS investigation of β-glucan oligosaccharide oxidation. The Analyst. 2016; 141(24): 6533-6548. doi: 10.1039/c6an01125j
94. Vuong TV, Vesterinen AH, Foumani M, et al. Xylo- and cello-oligosaccharide oxidation by gluco-oligosaccharide oxidase from Sarocladium strictumand variants with reduced substrate inhibition. Biotechnology for Biofuels. 2013; 6(1). doi: 10.1186/1754-6834-6-148
95. Dallinga JW, Heerma W. Reaction mechanism and fragment ion structure determination of deprotonated small oligosaccharides, studied by negative ion fast atom bombardment (tandem) mass spectrometry. Biological Mass Spectrometry. 1991; 20(4): 215-231. doi: 10.1002/bms.1200200410
96. Swanson KD, Worth AL, Glish GL. Use of an Open Port Sampling Interface Coupled to Electrospray Ionization for the On-Line Analysis of Organic Aerosol Particles. Journal of the American Society for Mass Spectrometry. 2017; 29(2): 297-303. doi: 10.1007/s13361-017-1776-y
97. Kraska U, Micheel F. Synthetische polysaccharide mit D-glucose und 3,6-anhydro-D-glucoseresten. Carbohydrate Research. 1976; 49: 195-199. doi: 10.1016/S0008-6215(00)83137-7
98. Kochetkov NK, Chizhov OS, Zolotarev BM. Mass-spectrometric study of carbohydrates. Chemistry of Natural Compounds. 1966; 2(3): 120-124. doi: 10.1007/bf01134228
99. Dufour A, Weng J, Jia L, et al. Revealing the chemistry of biomass pyrolysis by means of tunable synchrotron photoionisation-mass spectrometry. RSC Advances. 2013; 3(14): 4786. doi: 10.1039/c3ra40486b
100. Kim J, Yun E, Yu S, et al. Different Levels of Skin Whitening Activity among 3,6-Anhydro-l-galactose, Agarooligosaccharides, and Neoagarooligosaccharides. Marine Drugs. 2017; 15(10): 321. doi: 10.3390/md15100321
101. Chen C, Chen J, Geng Z, et al. Regioselectivity of oxidation by a polysaccharide monooxygenase from Chaetomium thermophilum. Biotechnology for Biofuels. 2018; 11(1). doi: 10.1186/s13068-018-1156-2
102. Fanuel M, Garajova S, Ropartz D, et al. The Podospora anserina lytic polysaccharide monooxygenase PaLPMO9H catalyzes oxidative cleavage of diverse plant cell wall matrix glycans. Biotechnology for Biofuels. 2017; 10(1). doi: 10.1186/s13068-017-0749-5
103. Bennati-Granier C, Garajova S, Champion C, et al. Substrate specificity and regioselectivity of fungal AA9 lytic polysaccharide monooxygenases secreted by Podospora anserina. Biotechnology for Biofuels. 2015; 8(1). doi: 10.1186/s13068-015-0274-3
104. Sun P, Frommhagen M, Kleine Haar M, et al. Mass spectrometric fragmentation patterns discriminate C1- and C4-oxidised cello-oligosaccharides from their non-oxidised and reduced forms. Carbohydrate Polymers. 2020; 234: 115917. doi: 10.1016/j.carbpol.2020.115917
105. Frommhagen M, van Erven G, Sanders M, et al. RP-UHPLC-UV-ESI-MS/MS analysis of LPMO generated C4-oxidized gluco-oligosaccharides after non-reductive labeling with 2-aminobenzamide. Carbohydrate Research. 2017; 448: 191-199. doi: 10.1016/j.carres.2017.03.006
106. Isaksen T, Westereng B, Aachmann FL, et al. A C4-oxidizing Lytic Polysaccharide Monooxygenase Cleaving Both Cellulose and Cello-oligosaccharides. Journal of Biological Chemistry. 2014; 289(5): 2632-2642. doi: 10.1074/jbc.m113.530196
107. Silva C de OG, Teixeira TS, Rodrigues KB, et al. Combination of MALDI-TOF MS and UHPLC-ESI-MS for the characterization of lytic polysaccharide monooxygenase activity. Analytical Methods. 2020; 12(2): 149-161. doi: 10.1039/c9ay01774g
108. Sun P, Laurent CVFP, Boerkamp VJP, et al. Regioselective C4 and C6 Double Oxidation of Cellulose by Lytic Polysaccharide Monooxygenases. ChemSusChem. 2021; 15(2). doi: 10.1002/cssc.202102203

109. Mudedla SK, Vuorte M, Veijola E, et al. Effect of oxidation on cellulose and water structure: a molecular dynamics simulation study. Cellulose. 2021; 28(7): 3917-3933. doi: 10.1007/s10570-021-03751-8
110. Westereng B, Arntzen MØ, Aachmann FL, et al. Simultaneous analysis of C1 and C4 oxidized oligosaccharides, the products of lytic polysaccharide monooxygenases acting on cellulose. Journal of Chromatography A. 2016; 1445: 46-54. doi: 10.1016/j.chroma.2016.03.064
111. Domon B, Costello CE. A systematic nomenclature for carbohydrate fragmentations in FAB-MS/MS spectra of glycoconjugates. Glycoconjugate Journal. 1988; 5(4): 397-409. doi: 10.1007/bf01049915
112. Stephens E, Maslen SL, Green LG, et al. Fragmentation Characteristics of Neutral N-Linked Glycans Using a MALDI-TOF/TOF Tandem Mass Spectrometer. Analytical Chemistry. 2004; 76(8): 2343-2354. doi: 10.1021/ac030333p
113. Spina E, Sturiale L, Romeo D, et al. New fragmentation mechanisms in matrix-assisted laser desorption/ionization time-of-flight/time-of-flight tandem mass spectrometry of carbohydrates. Rapid Communications in Mass Spectrometry. 2004; 18(4): 392-398. doi: 10.1002/rcm.1350
114. Moseley HNB, Rocca-Serra P, Salek RM, et al. InChI isotopologue and isotopomer specifications. Journal of Cheminformatics. 2024; 16(1). doi: 10.1186/s13321-024-00847-8
115. Romson J, Emmer Å. Mass calibration options for accurate electrospray ionization mass spectrometry. International Journal of Mass Spectrometry. 2021; 467: 116619. doi: 10.1016/j.ijms.2021.116619
116. Qiu L, Cooks RG. Pitfalls in Using Isotopic Distributions for Structural Interpretation by Mass Spectrometry. Journal of the American Society for Mass Spectrometry. 2024; 35(3): 642-645. doi: 10.1021/jasms.3c00457
117. Claesen J, Rockwood A, Gorshkov M, et al. The isotope distribution: A rose with thorns. Mass Spectrometry Reviews. 2023. doi: 10.1002/mas.21820
118. Satoh A. Introduction to practice of molecular simulation: Molecular dynamics, Monte Carlo, Brownian dynamics, lattice Boltzmann, dissipative particle dynamics. In: Elsevier insights Series. Elsevier, Amsterdam; 2011.
119. Ivanova B, Spiteller M. Experimental and theoretical mass spectrometric quantification of diffusion parameters and 3D structural determination of ions of L-tryptophyl-l-tryptophan in electrospray ionization conditions in positive operation mode. Journal of Molecular Structure. 2018; 1173: 848-864. doi: 10.1016/j.molstruc.2018.07.055
120. Ivanova B, Spiteller M. A mass spectrometric stochastic dynamic diffusion approach to selective quantitative and 3D structural analyses of native cyclodextrins by electrospray ionization and atmospheric pressure chemical ionization methods. Bioorganic Chemistry. 2019; 93: 103308. doi: 10.1016/j.bioorg.2019.103308
121. Ivanova B, Spiteller M. Mass spectrometric stochastic dynamic 3D structural analysis of mixture of steroids in solution – Experimental and theoretical study. Steroids. 2022; 181: 109001. doi: 10.1016/j.steroids.2022.109001

Appendix A

(Vibration spectroscopic data)

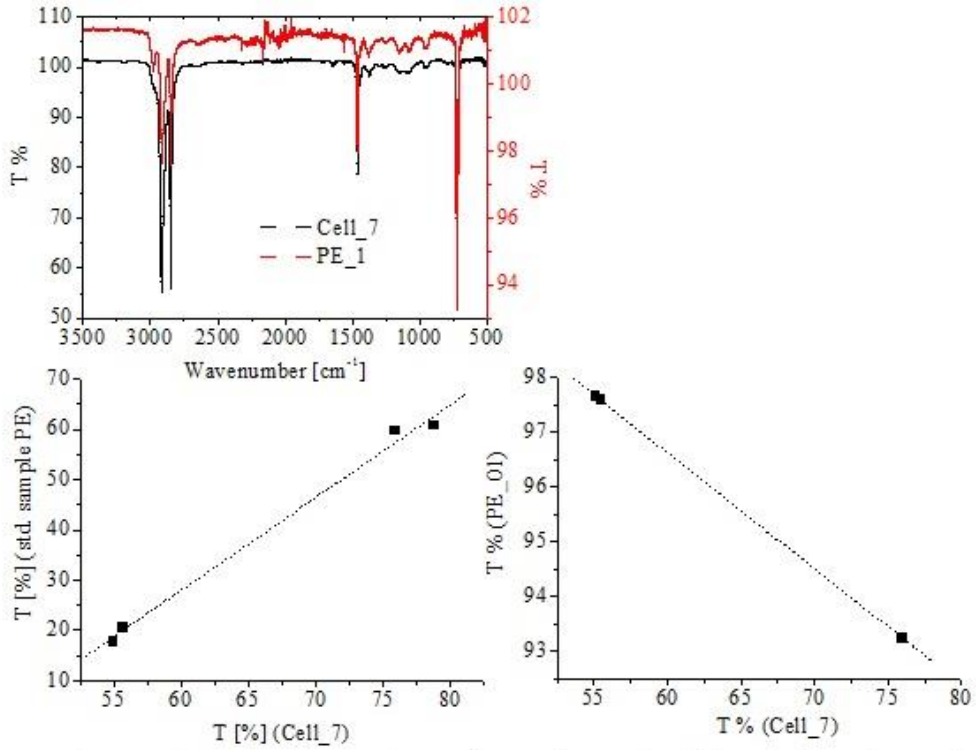

	Value	Error	
A	-82.78144	6.93397	
B	1.846	0.10308	
r	SD	N	*p*
0.9969	2.2829	4	0.0031

	Value	Error	
A	109.26297	0.01687	
B	-0.2108	$2.688.10^{-4}$	
r	SD	N	*p*
-1	0.0045	3	$8.1.10^{-4}$

Figure A1. FT-IR spectrum of samples Cell_7 and PE_01 [13] of cellulose and polyethylene; correlation between FT-IR bands of the analyte measured in transmission *T* [%] at 2915, 2846, 1465, and 722 cm^{-1} and standard sample of PE was according to [https://spectra.chem.ut.ee/paint/binders/polyethylene-wax/] and data on Cell_7 and PE_01 [13]; chemometrics.

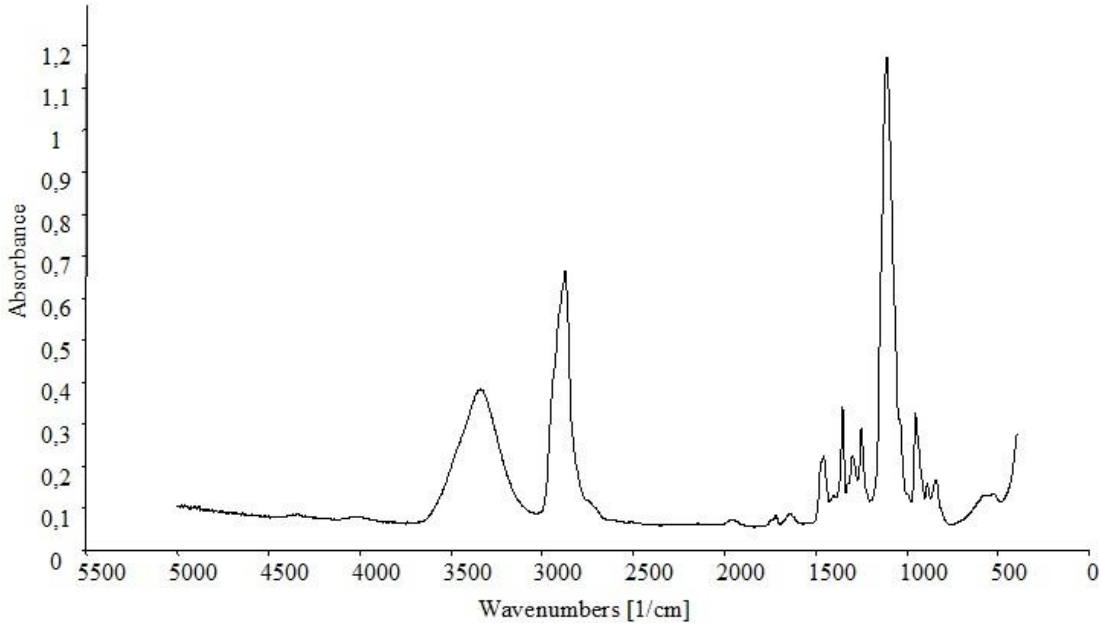

Figure A2. Solid-state FT-IR spectrum of standard sample of PEG within 5000–500 cm^{-1}.

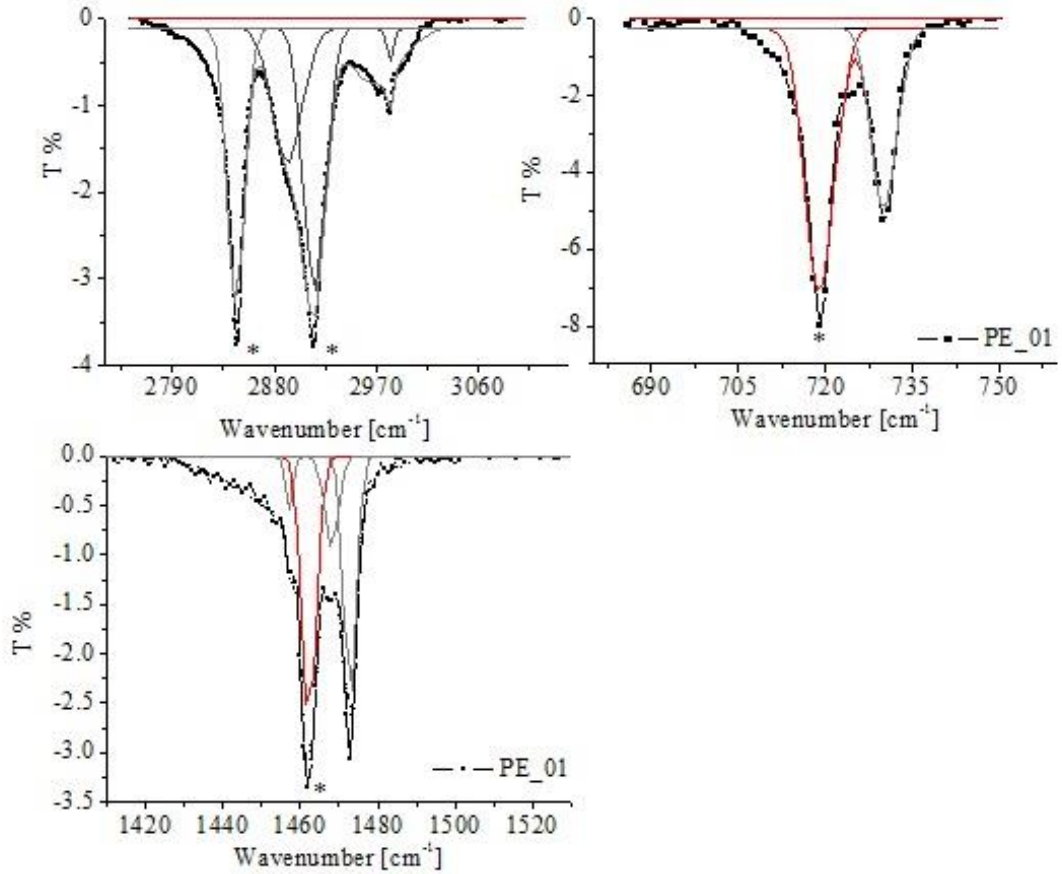

Figure A3. FT-IR spectra of samples PE_01 within different regions of the electromagnetic spectrum in transmission (*T*, %); curve-fitted FT-IR spectroscopic patterns.

Appendix B

(Mass spectrometric data)

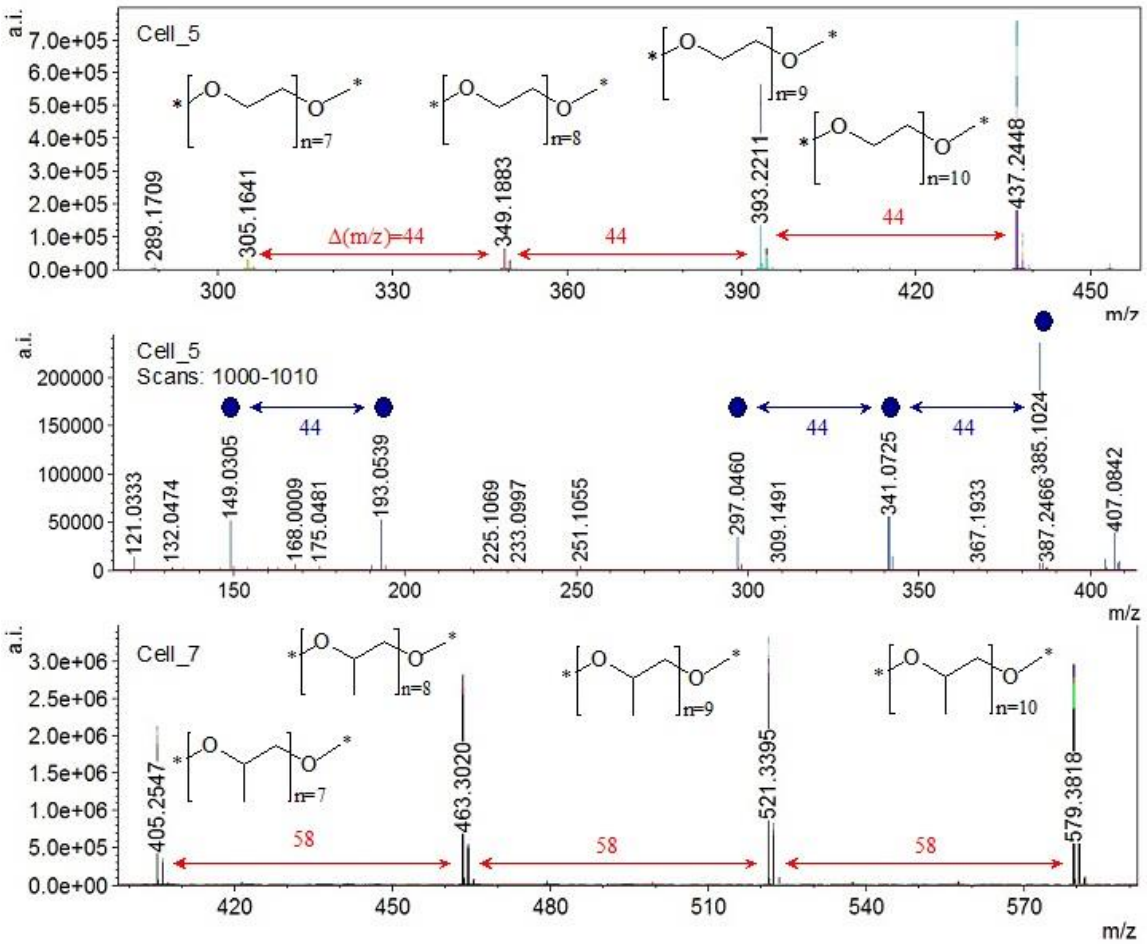

Figure B1. Mass spectra of Cell_5 sample in positive polarity per short spans of scan time; chemical diagrams of PEG and PPG polymer species.

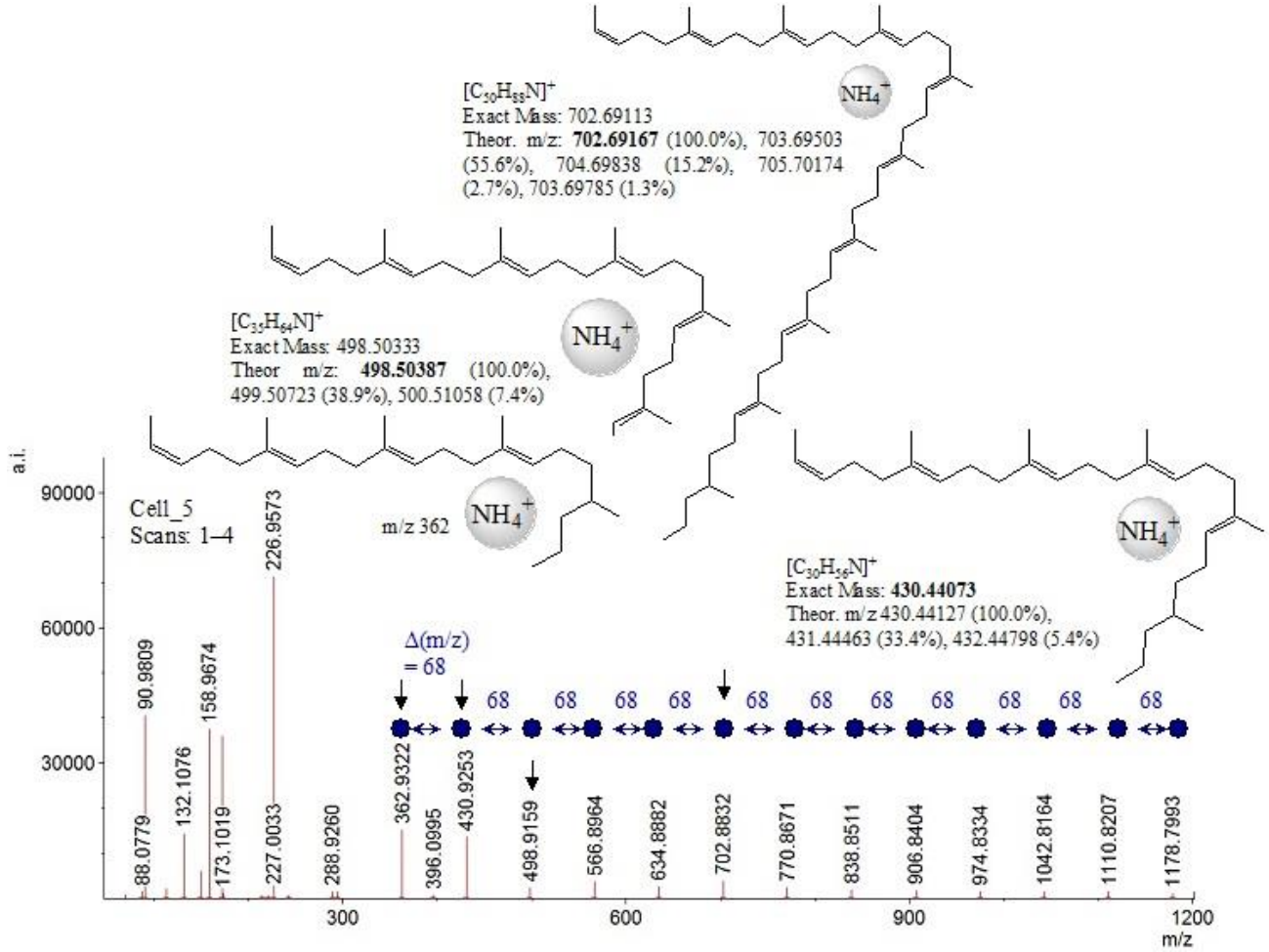

Figure B2. Mass spectra of Cell_5 sample in positive polarity per short spans of scan time (1.70–17.7 mins); chemical diagrams of ISOP polymer species.

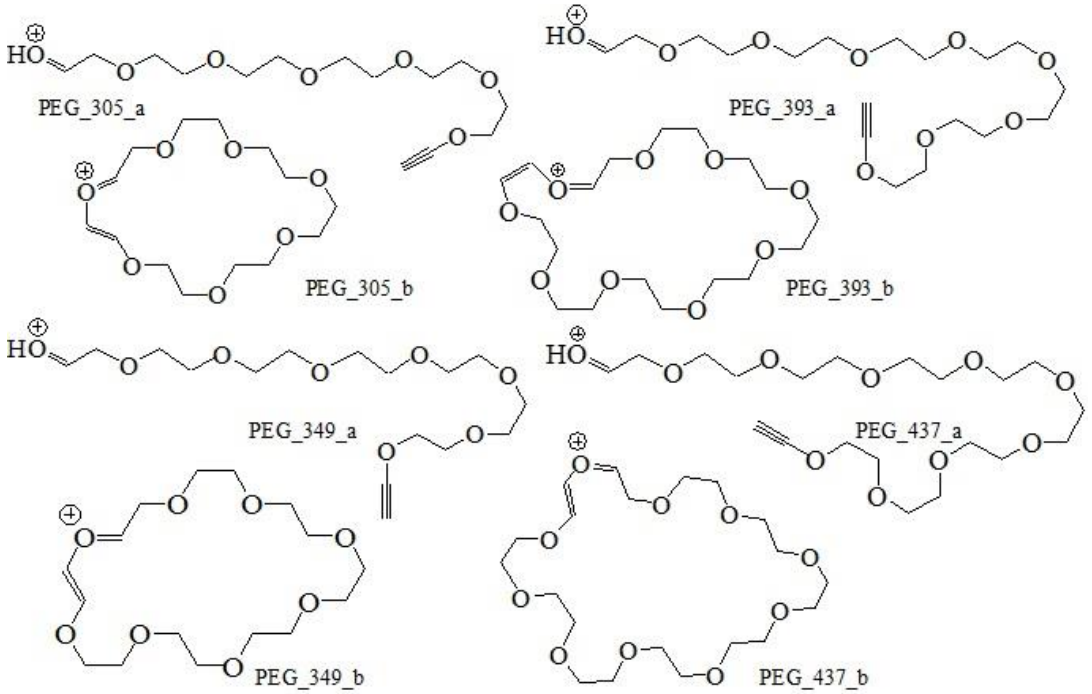

Figure B3. Chemical diagrams of product ions of PEG polymer.

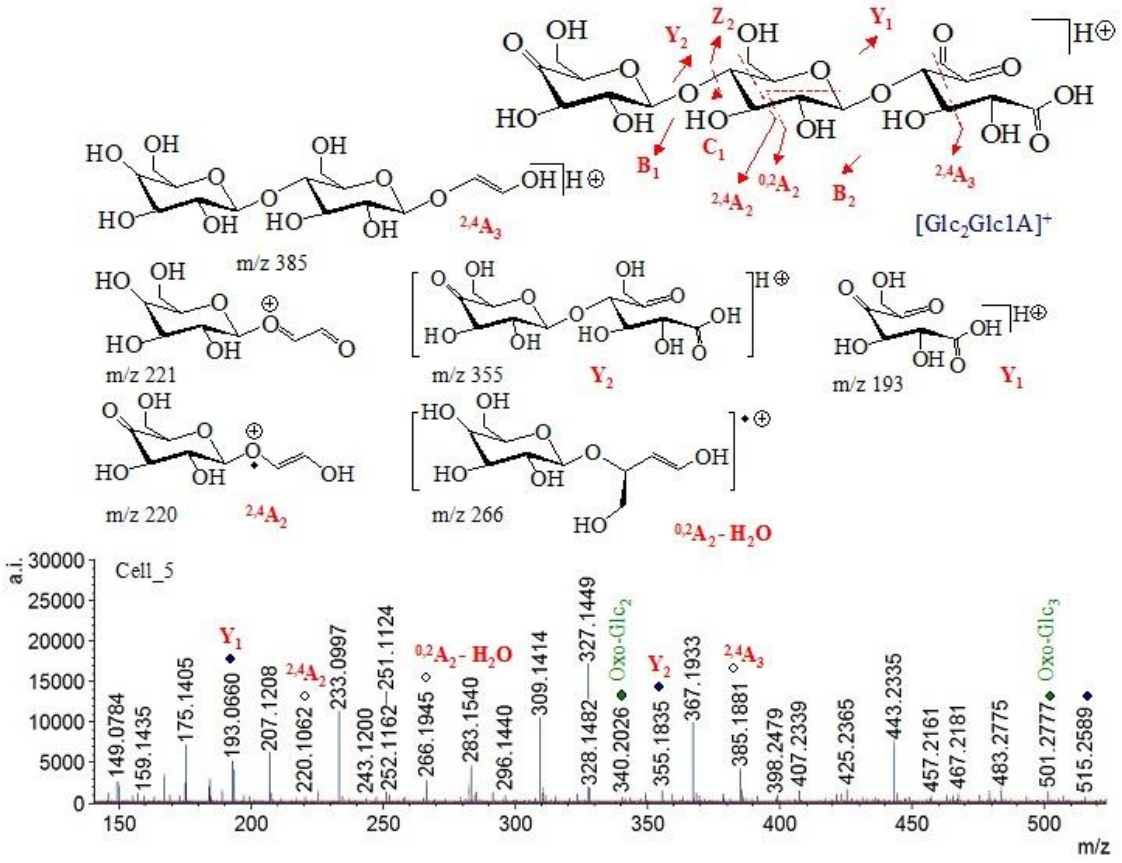

Figure B4. Mass spectrum of sample Cell_5 within m/z 100–550; chemical diagrams of observed carbohydrate species.

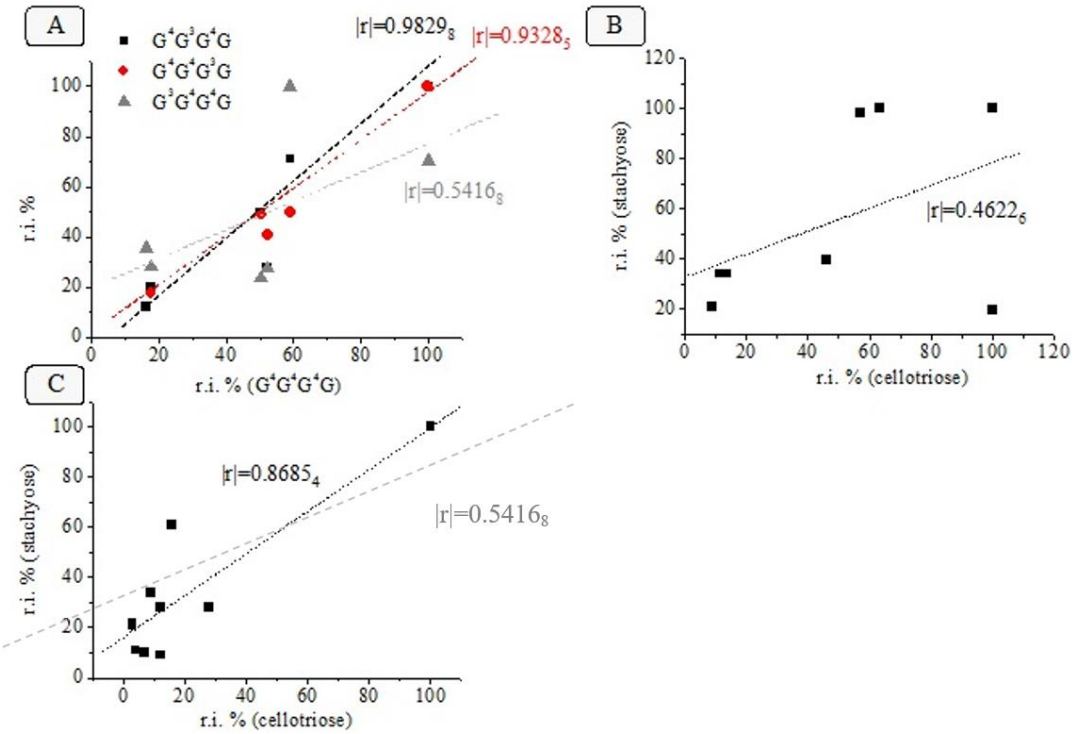

Figure B5. Functional relation between relative intensity data (r.i. %) of characteristic ions at m/z 655.21, 605.19, 503.16, 341.11, 179.06, and 161.05 of cellulose tetrameter depending on the positional β-1→3linked isomers [93]; the cello-isomer with only β-(1→4)-linkages is shown as $G^4G^4G^4G$, while 3G denotes carbohydrate monomer sub-units

having β-(1→3)-linkage **(A)**; correlative analysis between data on cellotriose and stachyose using characteristic ions at m/z 503, 443, 425, 383, 341, 283, 221, and 179 **(B)** as well as tandem mass spectrometric species of the common for the latter analytes peak at m/z 221 producing ions at m/z 203, 189, 161, 159, 131, 119, 113, 101, 89, and 71 **(C)** [95]; chemometrics.

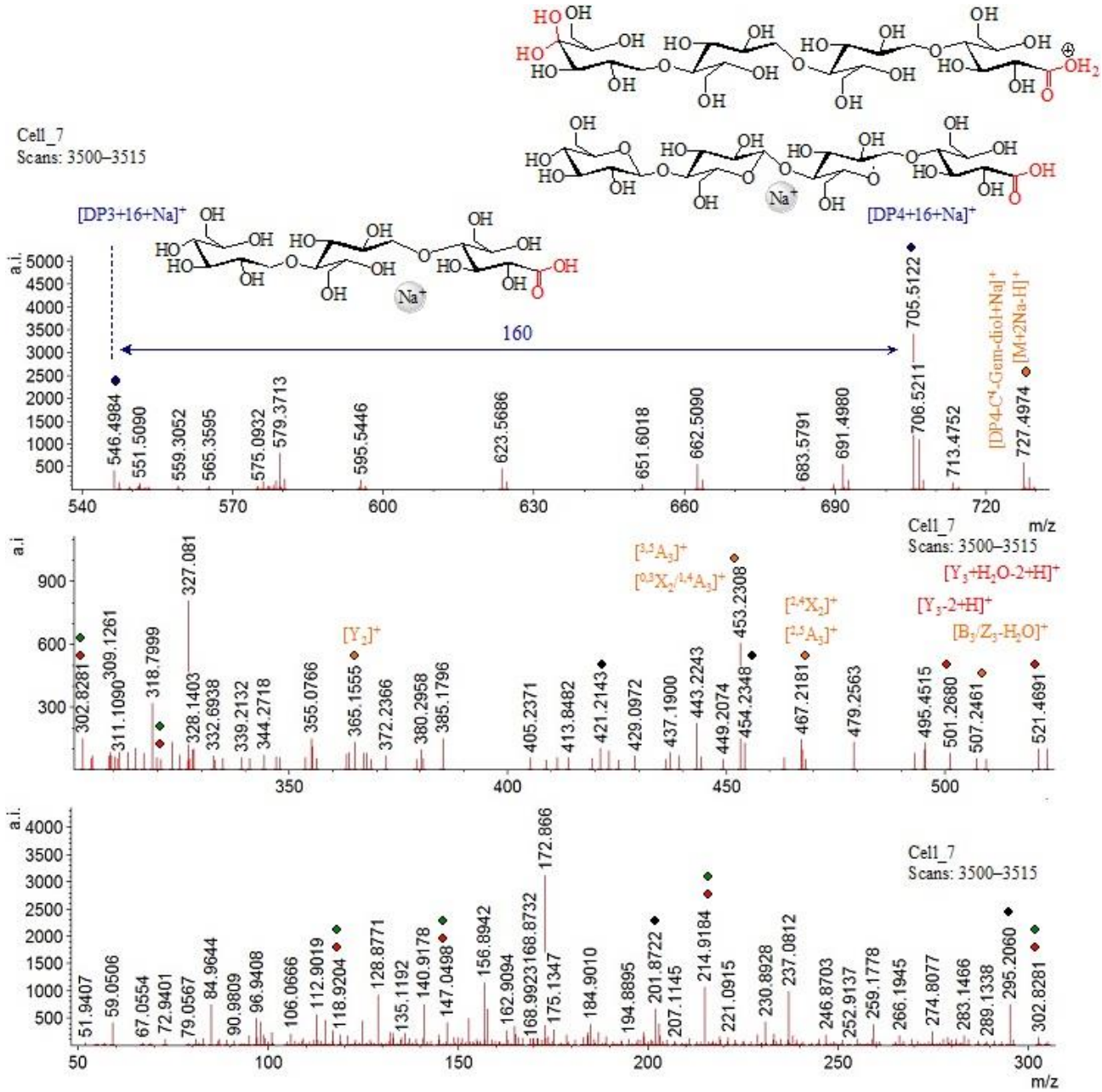

Figure B6. Mass spectrum of sample Cell_7 within m/z 50–800 and scan numbers 3500–3515 (RT = 41.09–41.23 mins); chemical diagrams of observed carbohydrate species.

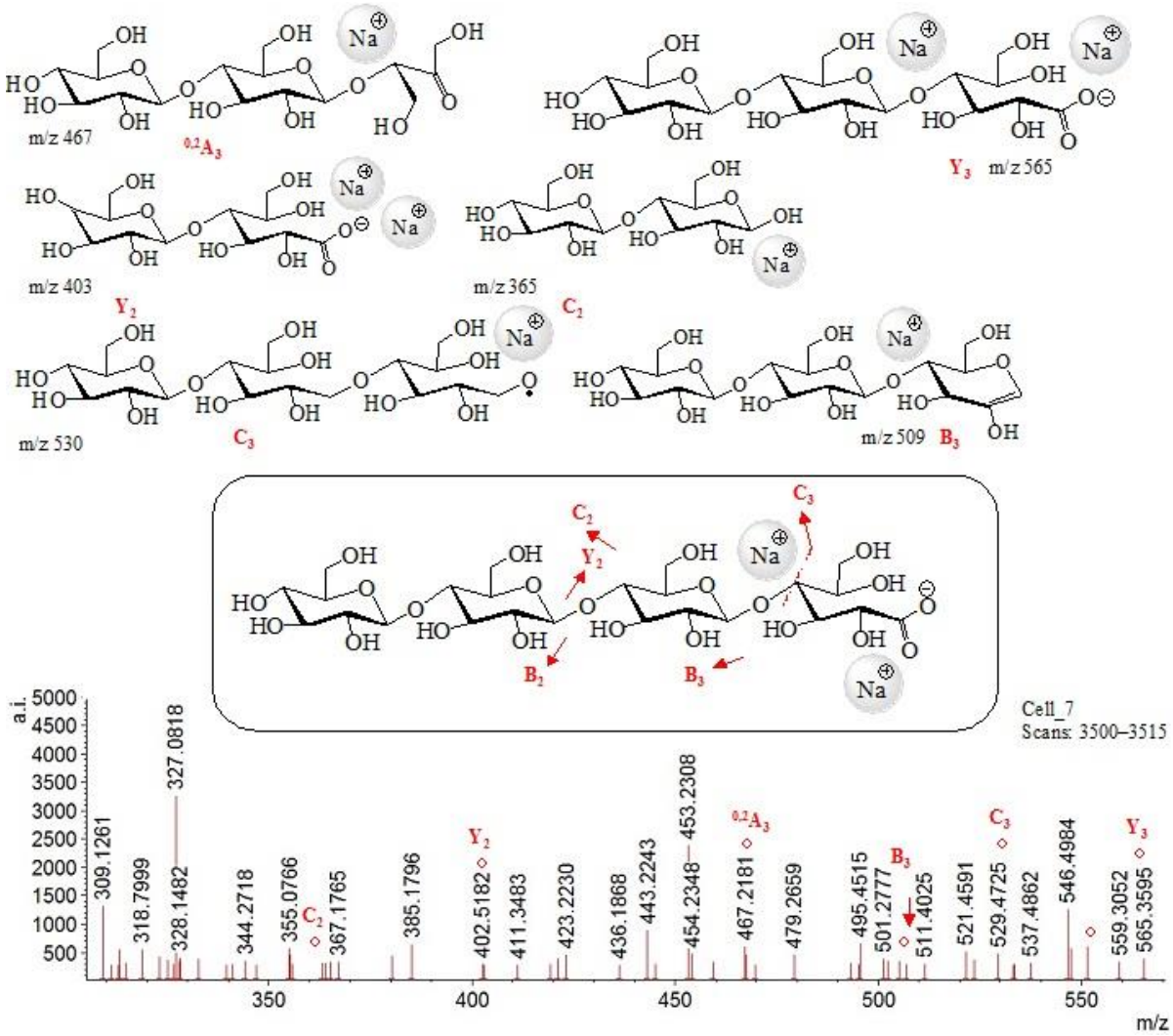

Figure B7. Mass spectrum of sample Cell_7 within m/z 300–600 and scan numbers 3500–3515 (RT = 41.09–41.23 mins); chemical diagrams of observed carbohydrate species.

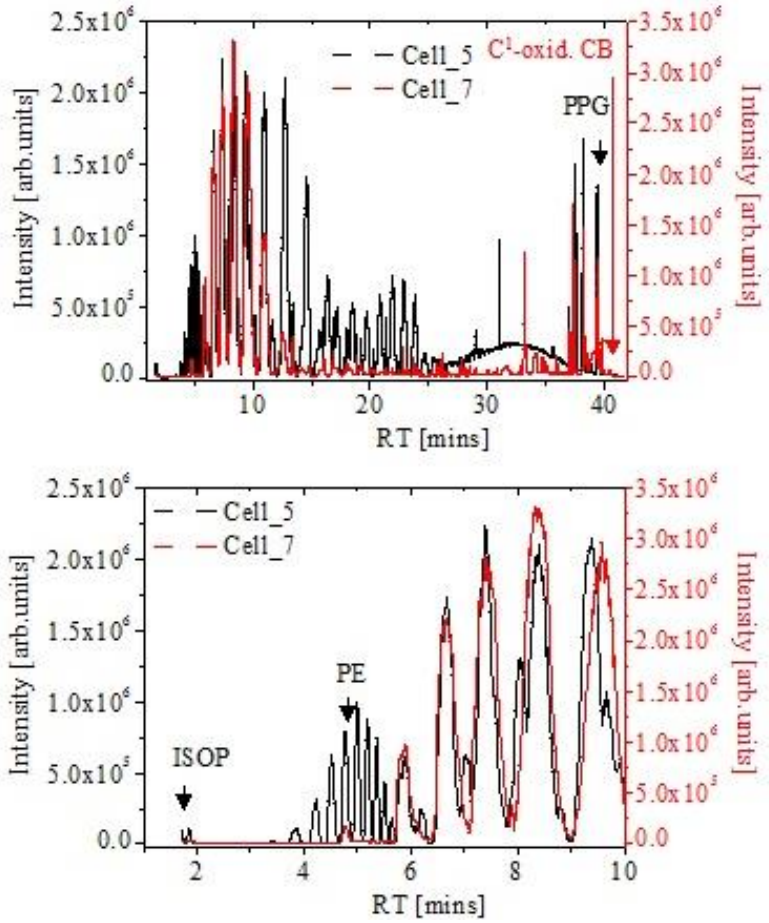

Figure B8. Chromatographic data on Cell_5 and Cell_7; peaks of analytes and highlighted.

Appendix C

(Theoretical data)

$$x - \langle x \rangle = \left(\sqrt{-2 \times \sigma \times \sigma \times \ln P1}\right) \times \sin(2 \times \pi \times P2) \quad \text{(C1)}$$

$$(x - \langle x \rangle) \times (x - \langle x \rangle) = (-2 \times \sigma \times \sigma \times \ln P1) \times \sin(2 \times \pi \times P2) \times \sin(2 \times \pi \times P2) \quad \text{(C2)}$$

$$\sigma \times \sigma = \langle x \times x \rangle - \langle x \rangle \times \langle x \rangle \text{ or } \sigma \times \sigma = \langle (x - \langle x \rangle) \times (x - \langle x \rangle) \rangle \quad \text{(C3)}$$

$$\ln P1 = (\langle (I - \langle I \rangle) \times (I - \langle I \rangle) \rangle / (0.5864 \times \sigma \times \sigma) \quad \text{(C4)}$$

$$A/(2 \times \sigma' \times \sigma') = 5.8639 \times 10^2 \times (\langle (x - \langle x \rangle) \times (x - \langle x \rangle) \rangle / \langle x \times x \rangle - \langle x \rangle \times \langle x \rangle) \quad \text{(C5)}$$

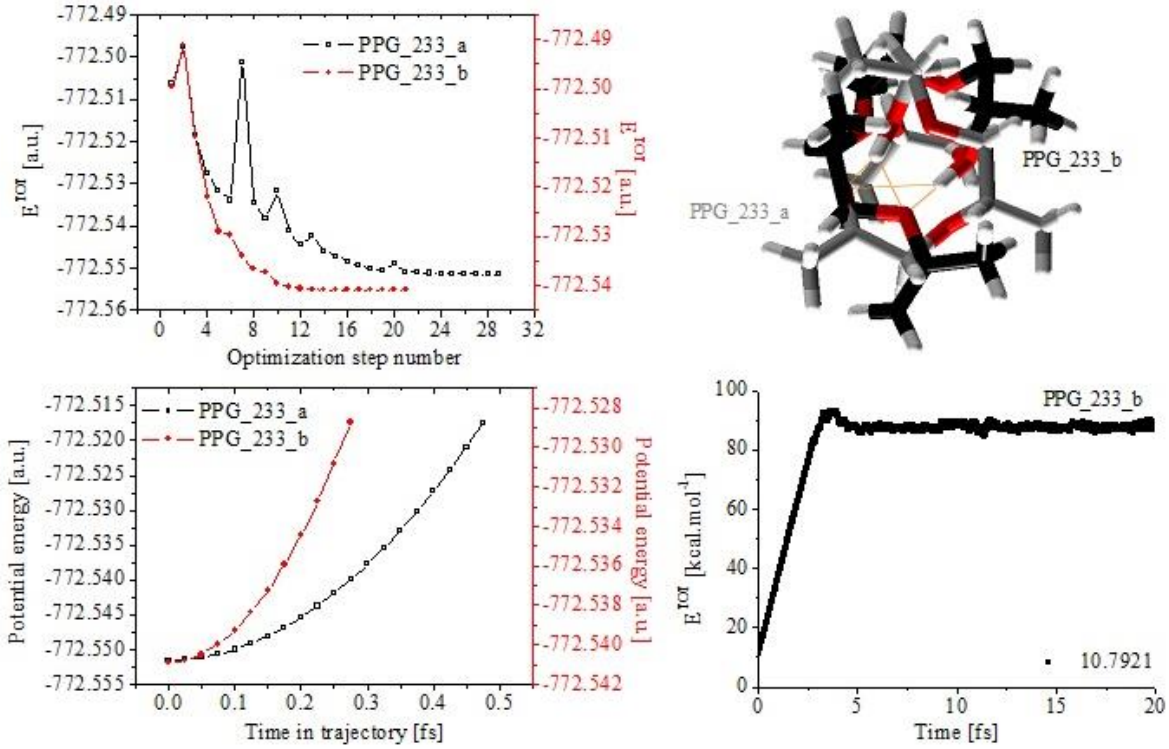

Figure C1. Static and molecular dynamics (BOMD and MM2/MD) data on cations PPG_233_a and PPG_233_b of PPG assigned as models to mass spectrometric peak at m/z 233; total energy (E^{TOT}) [a.u.] with respect to optimisation step number; MM2/MD: Total energy (E^{TOT} [kcal mol^{-1}]) versus time [fs]; and BOMD: Potential energy [a.u.] versus time in trajectory [fs]; optimised 3D molecular and electronic structures of the species at M062X/SDD level of theory.

Table C1. Thermochemistry (M062X/SDD) of observable mass spectrometric ions in ground and transition states in gas-phase, depending on theoretical level of computations and ionic structures; theoretical intensity (I^{Theor}_{SD}) data on Equation (4)).

	m/z 59		**m/z 59**		**m/z 117**	
	PPG_59_a		**PPG_59_b**		**PPG_117_a**	
	M062X/SDD		**M062X/SDD**		**M062X/SDD**	
	GS	**TS**	**GS**	**TS**	**GS**	**TS**
E_{ZPVE}	61.21540	61.06519	60.99972	60.49114	118.14850	117.99449
E_{corr}	0.102848	0.101923	0.102830	0.101529	0.198415	0.197389
H_{corr}	0.103792	0.102868	0.103774	0.102473	0.199359	0.198333
G_{corr}	0.069883	0.070420	0.069557	0.069258	0.152541	0.153466
ε_0	0.097553	0.097314	0.097209	0.096399	0.188282	0.188036

Table C1. (*Continued*).

	m/z 59		**m/z 59**		**m/z 117**	
	PPG_59_a		**PPG_59_b**		**PPG_117_a**	
	M062X/SDD		**M062X/SDD**		**M062X/SDD**	
	GS	**TS**	**GS**	**TS**	**GS**	**TS**
E	−193.247615	−193.248121	−193.215590	−193.212718	−386.213343	−386.214006
H	−193.246671	−193.247177	−193.214646	−193.211774	−386.212399	−386.213061
G	−193.280580	−193.279624	−193.248864	−193.244989	−386.259217	−386.257928
D_{QC}	123.45295		250.9667		72.7582	
I^{Theor}_{SD}	5.702196×10^{-8}		8.1379×10^{8}		4.3822×10^{-8}	
	m/z 117		**m/z 175**		**m/z 175**	
	PPG_117_b		**PPG_175_a**		**PPG_175_b**	
	M062X/SDD		**M062X/SDD**		**M062X/SDD**	
	GS	**TS**	**GS**	**TS**	**GS**	**TS**
E_{ZPVE}	133.76380	133.58718	175.06494	175.07570	174.59420	174.01772
E_{corr}	0.223641	0.222771	0.293717	0.293125	0.292733	0.291460
H_{corr}	0.224585	0.223715	0.294661	0.294070	0.293677	0.292405
G_{corr}	0.177492	0.177963	0.236807	0.237871	0.236675	0.235883
ε_0	0.213166	0.212885	0.278984	0.279001	0.278234	0.277315
E	−387.413844	−387.412155	−579.204835	−579.202845	−579.179905	−579.177164
H	−387.412900	−387.411211	−579.203891	−579.201901	−579.178961	−579.176220
G	−387.459993	−387.456963	−579.261745	−579.258100	−579.235963	−579.232741
D_{QC}	149.2742		97.88136		415.2433	
I^{Theor}_{SD}	6.2762×10^{-8}		5.0822×10^{-8}		1.04677×10^{-7}	
	m/z 233		**m/z 233**			
	PPG_233_a		**PPG_233_b**			
	M062X/SDD		**M062X/SDD**			
	GS	**TS**	**GS**	**TS**		
E_{ZPVE}	232.28117	232.10746	233.34975	232.92663		
E_{corr}	0.389410	0.388381	0.390574	0.389555		
H_{corr}	0.390354	0.389325	0.391518	0.390499		
G_{corr}	0.323322	0.324160	0.325811	0.325097		
ε_0	0.370164	0.369887	0.371866	0.371192		
E	−772.162155	−772.161638	−772.150329	−772.143173		
H	−772.161211	−772.160694	−772.149384	−772.142228		
G	−772.228243	−772.225859	−772.215091	−772.207631		
D_{QC}	79.41055		556.8518			
I^{Theor}_{SD}	4.57787×10^{-8}		1.2122×10^{-7}			

E_{ZPVE}—zero-point vibration energy [kcal/mol]; ε_0—zero-point correction [Hartree/partice]; E_{corr}—thermal correction to energy [Hartree/partice]; H_{corr}—thermal correction to enthalpy [Hartree/partice]; G_{corr}—thermal correction to free energy [Hartree/partice]; E—sum of electronic and thermal energies [Hartree/partice]; H—sum of electronic and thermal enthalpies [Hartree/partice]; G—sum of electronic and thermal free energies [Hartree (partice)$^{-1}$]

Table C2. Atomic co-ordinates of mass spectrometric product ions of PPG used to compute the energetics summarised in **Table C1** and the vibration modes listed in **Table C3** in ground and transition states.

PPG_175_a (GS)				**PPG_175_a (TS)**			
Atom	***x***	***y***	***z***	**Atom**	***x***	***y***	***z***
O	−1.040547	−1.429567	−0.461319	O	−1.05192	−1.41817	−0.45637
C	−2.185364	−1.02765	−0.137412	C	−2.15435	−1.01111	−0.13903
C	−3.38804	−1.89552	−0.311657	C	−3.35473	−1.88891	−0.30182
C	−2.347179	0.358388	0.469456	C	−2.32686	0.37951	0.48158
O	−1.073465	0.926843	0.782585	O	−1.0455	0.93957	0.78555
C	−0.368679	1.655019	−0.278525	C	−0.34072	1.66774	−0.27557
C	1.077901	1.190198	−0.166186	C	1.10586	1.20292	−0.16323
C	−0.495111	3.158485	−0.059004	C	−0.46715	3.17121	−0.05604
O	1.093117	−0.258072	−0.432753	O	1.12108	−0.24535	−0.42979
C	2.30966	−1.092042	−0.10779	C	2.33762	−1.07932	−0.10483
C	2.407757	−1.263815	1.403978	C	2.43572	−1.25109	1.40694
C	3.526773	−0.443669	−0.751384	C	3.55473	−0.43094	−0.74842
H	0.127108	−0.763701	−0.38517	H	0.15507	−0.75098	−0.38221
H	−3.226033	−2.624975	−1.106161	H	−3.19807	−2.61225	−1.1032
H	−4.285028	−1.303024	−0.509984	H	−4.25707	−1.2903	−0.50702
H	−3.558651	−2.446386	0.623089	H	−3.53069	−2.43366	0.62605
H	−2.912414	0.274027	1.403289	H	−2.88445	0.28675	1.40625
H	−2.940119	0.980799	−0.21817	H	−2.91216	0.99352	−0.21521
H	−0.773738	1.367574	−1.261268	H	−0.74578	1.3803	−1.25831
H	1.446526	1.364808	0.848809	H	1.47449	1.37753	0.85177
H	1.718033	1.674402	−0.905047	H	1.74599	1.68713	−0.90209
H	−1.546659	3.45709	−0.088431	H	−1.5187	3.46982	−0.08547
H	0.039016	3.717314	−0.833767	H	0.06698	3.73004	−0.83081
H	−0.094652	3.429907	0.921692	H	−0.06669	3.44263	0.92465
H	2.069985	−2.038452	−0.59949	H	2.09795	−2.02573	−0.59653
H	1.472923	−1.645734	1.824429	H	1.50088	−1.63301	1.82739
H	2.666104	−0.323826	1.901367	H	2.69407	−0.3111	1.90433
H	3.200688	−1.983578	1.628549	H	3.22865	−1.97085	1.63151
H	4.380927	−1.118989	−0.647425	H	4.40889	−1.10626	−0.64447
H	3.791789	0.495939	−0.25585	H	3.81975	0.50866	−0.25289
H	3.365054	−0.263195	−1.817424	H	3.39302	−0.25047	−1.81446
PPG_59_a (GS)				**PPG_59_a (TS)**			
Atom	***x***	***y***	***z***	**Atom**	***x***	***y***	***z***
O	0.016803	1.3504	0.004072	O	−0.0243	1.29397	−0.0012
C	−0.003666	0.05291	0.001065	C	−0.00144	0.00162	−0.00476
C	−1.346917	−0.560877	0.008134	C	1.3441	−0.6221	−0.00037
C	1.247234	−0.744753	−0.005779	C	−1.26303	−0.79146	0.01584
H	0.874308	1.83823	−0.024926	H	−0.88247	1.78312	0.02582
H	−1.350177	−1.491585	0.581109	H	1.34201	−1.5467	−0.58022

Table C2. (*Continued*).

PPG_59_a (GS)				**PPG_59_a (TS)**			
Atom	***x***	***y***	***z***	**Atom**	***x***	***y***	***z***
H	−1.598372	−0.832243	−1.030663	H	1.59021	−0.88736	1.03156
H	−2.105689	0.135255	0.366536	H	2.09753	0.08014	−0.36564
H	2.136273	−0.169631	−0.274478	H	−2.14444	−0.22474	0.27537
H	1.139947	−1.605001	−0.673828	H	−1.14811	−1.66011	0.67472
H	1.389382	−1.161905	1.00316	H	−1.39755	−1.21701	−1.00227
PPG_59_b (GS)				**PPG_59_b (TS)**			
Atom	***x***	***y***	***z***	**Atom**	***x***	***y***	***z***
O	0.858111	−1.033651	−0.0003	O	0.83431	−1.0388	0.00675
C	−0.039326	0.206749	−0.000502	C	−0.05475	0.21959	−0.01643
C	−1.480666	−0.174809	0.002551	C	−1.48807	−0.19671	0.02671
C	0.635602	1.350537	−0.002691	C	0.58276	1.37942	0.02949
H	1.143442	−1.444494	0.842055	H	1.11734	−1.44502	0.84218
H	1.075316	−1.493686	−0.837599	H	1.0492	−1.4942	−0.83749
H	−2.083731	0.735701	0.004327	H	−2.10982	0.73514	0.00444
H	−1.744756	−0.755269	0.891967	H	−1.77087	−0.75581	0.89211
H	−1.749617	−0.753067	−0.887079	H	−1.77572	−0.75359	−0.88696
H	0.081765	2.28314	0.000808	H	0.05561	2.28268	0.00092
H	1.719033	1.402017	−0.008219	H	1.69288	1.40151	−0.00811
PPG_117_a (GS)				**PPG_117_a (TS)**			
Atom	***x***	***y***	***z***	**Atom**	***x***	***y***	***z***
O	−1.69842	−1.30162	0.32438	O	−1.69842	−1.30162	0.32438
C	−1.88788	−0.06435	0.01482	C	−1.88788	−0.06435	0.01482
C	−3.25814	0.47604	−0.06624	C	−3.25814	0.47604	−0.06624
C	−0.62228	0.71997	−0.23182	C	−0.62228	0.71997	−0.23182
O	0.40582	−0.24918	−0.02057	O	0.40582	−0.24918	−0.02057
C	1.8105	0.10515	−0.38456	C	1.8105	0.10515	−0.38456
C	2.62246	−1.14641	−0.08946	C	2.62246	−1.14641	−0.08946
C	2.26171	1.3231	0.41606	C	2.26171	1.3231	0.41606
H	−0.69956	−1.5155	0.33839	H	−0.69956	−1.5155	0.33839
H	−3.99952	−0.29105	0.15457	H	−3.99952	−0.29105	0.15457
H	−3.43455	0.89049	−1.06704	H	−3.43455	0.89049	−1.06704
H	−3.36688	1.31362	0.63476	H	−3.36688	1.31362	0.63476
H	−0.57502	1.56289	0.47177	H	−0.57502	1.56289	0.47177
H	−0.63151	1.1258	−1.2547	H	−0.63151	1.1258	−1.2547
H	1.80163	0.31935	−1.46136	H	1.80163	0.31935	−1.46136
H	2.23764	−2.00804	−0.64166	H	2.23764	−2.00804	−0.64166
H	2.60504	−1.36847	0.98177	H	2.60504	−1.36847	0.98177
H	3.66204	−0.98811	−0.38922	H	3.66204	−0.98811	−0.38922
H	1.69968	2.22855	0.16204	H	1.69968	2.22855	0.16204

Table C2. (*Continued*).

PPG_117_a (GS)				**PPG_117_a (TS)**			
Atom	***x***	***y***	***z***	**Atom**	***x***	***y***	***z***
H	3.31388	1.52772	0.19824	H	3.31388	1.52772	0.19824
H	2.16967	1.12814	1.48919	H	2.16967	1.12814	1.48919
PPG_117_b (GS)				**PPG_117_b (TS)**			
Atom	***x***	***y***	***z***	**Atom**	***x***	***y***	***z***
O	1.56208	1.338087	−0.039153	O	1.54693	1.31486	−0.02913
C	1.914605	−0.038713	−0.409279	C	1.90544	−0.04908	−0.41567
C	3.161464	−0.539705	0.305514	C	3.15803	−0.5749	0.32776
C	0.651893	−0.807341	0.028092	C	0.616	−0.80626	0.05606
O	−0.455269	0.160743	−0.189956	O	−0.47207	0.14083	−0.18489
C	−1.841485	−0.058496	0.40913	C	−1.85829	−0.07841	0.41419
C	−2.388879	−1.343723	−0.187467	C	−2.40568	−1.36364	−0.18241
C	−2.636238	1.189337	0.058014	C	−2.65304	1.16942	0.06308
H	2.264793	2.003791	−0.14957	H	2.24799	1.98387	−0.14451
H	−0.012366	1.082457	−0.13141	H	−0.02917	1.06254	−0.12635
H	2.027447	−0.087789	−1.496691	H	2.01065	−0.10771	−1.49164
H	3.066454	−0.398571	1.386161	H	3.04965	−0.41849	1.39123
H	4.051471	−0.007286	−0.041308	H	4.03467	−0.02721	−0.03624
H	3.318167	−1.604248	0.102616	H	3.30137	−1.62418	0.10768
H	0.673374	−1.053082	1.094604	H	0.65657	−1.073	1.09968
H	0.459635	−1.687414	−0.582424	H	0.44283	−1.70732	−0.57735
H	−1.668841	−0.144641	1.488119	H	−1.68564	−0.16456	1.49318
H	−2.4351	−1.272015	−1.277715	H	−2.4519	−1.29193	−1.27265
H	−3.404916	−1.496466	0.187946	H	−3.42172	−1.51638	0.19301
H	−1.802818	−2.222121	0.097369	H	−1.81962	−2.24204	0.10243
H	−2.1808	2.097757	0.465353	H	−2.1976	2.07784	0.47041
H	−3.636345	1.102607	0.491626	H	−3.65315	1.08269	0.49669
H	−2.742803	1.288223	−1.02582	H	−2.7596	1.2683	−1.02076
PPG_233_a (GS)				**PPG_233_a (TS)**			
Atom	***x***	***y***	***z***	**Atom**	***x***	***y***	***z***
O	0.493092	−1.717278	−0.286253	O	0.48475	−1.70868	−0.29286
C	1.714648	−1.528214	−0.484053	C	1.71109	−1.50933	−0.50379
C	2.68129	−2.667003	−0.378394	C	2.68232	−2.66797	−0.37522
C	2.265658	−0.169638	−0.865351	C	2.24072	−0.14159	−0.85759
O	1.30161	0.876436	−0.759193	O	1.29194	0.88768	−0.76977
C	1.461054	1.822553	0.358736	C	1.45138	1.8338	0.34816
C	0.215079	1.716215	1.222222	C	0.20541	1.72746	1.21165
C	1.652826	3.222575	−0.211781	C	1.64316	3.23382	−0.22235
O	0.150464	0.347215	1.691375	O	0.1408	0.35846	1.6808
C	−1.133481	−0.107152	2.19408	C	−1.14315	−0.09591	2.18351

Table C2. (*Continued*).

PPG_233_a (GS)				**PPG_233_a (TS)**			
Atom	***x***	***y***	***z***	**Atom**	***x***	***y***	***z***
C	−0.920935	−1.524277	2.71668	C	−0.9306	−1.51303	2.70611
C	−2.186281	−0.03545	1.069318	C	−2.19595	−0.0242	1.05874
O	−1.557649	−0.465263	−0.184116	O	−1.56732	−0.45402	−0.19469
C	−2.231644	−0.152267	−1.485509	C	−2.24131	−0.14102	−1.49608
C	−1.607533	−1.067752	−2.531601	C	−1.6172	−1.05651	−2.54217
C	−2.048344	1.327562	−1.805549	C	−2.05801	1.33881	−1.81612
H	−0.539614	−0.911381	−0.20567	H	−0.54928	−0.90013	−0.21624
H	3.070243	−2.696096	0.648012	H	3.06058	−2.68485	0.63745
H	3.533453	−2.536924	−1.050496	H	3.52379	−2.52568	−1.06107
H	2.180568	−3.615626	−0.575811	H	2.1709	−3.60438	−0.58638
H	2.593238	−0.242533	−1.912734	H	2.58357	−0.23128	−1.9233
H	3.166313	0.019488	−0.263578	H	3.15664	0.03074	−0.27415
H	2.328518	1.517362	0.959352	H	2.31885	1.52861	0.94878
H	−0.657892	1.970508	0.605689	H	−0.66756	1.98176	0.59512
H	0.270803	2.410631	2.069919	H	0.26113	2.42188	2.05935
H	2.552994	3.264093	−0.829934	H	2.54332	3.27534	−0.84051
H	1.750177	3.961094	0.590508	H	1.74051	3.97234	0.57993
H	0.797466	3.495267	−0.838398	H	0.7878	3.50652	−0.84897
H	−1.47408	0.548479	3.008001	H	−1.48375	0.55973	2.99743
H	−0.642298	−2.203676	1.904974	H	−0.65196	−2.19243	1.8944
H	−1.8311	−1.898605	3.194458	H	−1.84077	−1.88736	3.18388
H	−0.116907	−1.521559	3.455807	H	−0.12657	−1.51031	3.44523
H	−2.560832	0.979457	0.912827	H	−2.5705	0.9907	0.90225
H	−3.024706	−0.705577	1.278833	H	−3.03437	−0.69433	1.26826
H	−3.283077	−0.409057	−1.319223	H	−3.29275	−0.39781	−1.3298
H	−2.161371	−0.967741	−3.468979	H	−2.17104	−0.9565	−3.47955
H	−1.643	−2.115109	−2.220068	H	−1.65267	−2.10386	−2.23064
H	−0.568208	−0.778329	−2.722162	H	−0.57788	−0.76708	−2.73274
H	−2.515154	1.543844	−2.771628	H	−2.52482	1.55509	−2.7822
H	−0.98014	1.559363	−1.872974	H	−0.98981	1.57061	−1.88355
H	−2.51956	1.980832	−1.064021	H	−2.52923	1.99208	−1.07459
PPG_233_b (GS)				**PPG_233_b (TS)**			
Atom	***x***	***y***	***z***	**Atom**	***x***	***y***	***z***
O	0.030449	1.233154	−0.636831	O	0.03641	1.23212	−0.60878
C	−0.646533	1.815328	0.559276	C	−0.6298	1.83743	0.55779
C	−0.084575	3.194263	0.847728	C	−0.05753	3.1717	0.89777
C	−2.14966	1.832358	0.174443	C	−2.18103	1.87508	0.2348
O	−2.37881	0.776057	−0.796366	O	−2.37582	0.78098	−0.77724
C	−2.988571	−0.484766	−0.348907	C	−2.98558	−0.47984	−0.32978
C	−2.080761	−1.170196	0.680982	C	−2.07777	−1.16527	0.70011

Table C2. (*Continued*).

PPG_233_b (GS)				**PPG_233_b (TS)**			
Atom	***x***	***y***	***z***	**Atom**	***x***	***y***	***z***
C	−3.188816	−1.315942	−1.608035	C	−3.18583	−1.31102	−1.58891
O	−0.750763	−1.184501	0.108253	O	−0.74777	−1.17958	0.12738
C	0.268196	−2.004333	0.749072	C	0.27118	−1.99941	0.7682
C	0.504029	−1.625862	2.212615	C	0.50702	−1.62094	2.23174
C	1.503216	−1.803656	−0.119785	C	1.5062	−1.79873	−0.10066
O	1.817899	−0.368796	−0.15117	O	1.82089	−0.36387	−0.13205
C	3.129693	0.048855	−0.555544	C	3.13268	0.05378	−0.53642
C	3.321543	1.505281	−0.253779	C	3.32453	1.5102	−0.23466
C	4.002372	−0.791675	−1.120231	C	4.00536	−0.78675	−1.10111
H	−0.710188	0.793548	−1.169293	H	−0.7072	0.79848	−1.15016
H	0.824912	0.525887	−0.412674	H	0.82791	0.5308	−0.39354
H	−0.460473	1.111514	1.376924	H	−0.4575	1.11647	1.396
H	−0.172722	3.830551	−0.037275	H	−0.16971	3.83542	−0.01807
H	0.966588	3.146115	1.143356	H	0.96966	3.15103	1.16251
H	−0.644545	3.65848	1.666876	H	−0.64155	3.66339	1.68601
H	−2.400191	2.769988	−0.326524	H	−2.39723	2.77496	−0.30741
H	−2.778589	1.717165	1.063109	H	−2.77567	1.72208	1.08234
H	−3.951942	−0.248462	0.120349	H	−3.94895	−0.24354	0.13947
H	−2.441551	−2.190418	0.86874	H	−2.43856	−2.18549	0.88786
H	−2.076353	−0.621675	1.634113	H	−2.07336	−0.61675	1.65324
H	−3.752795	−0.742784	−2.346603	H	−3.74981	−0.73786	−2.32748
H	−3.745629	−2.228763	−1.376497	H	−3.74264	−2.22384	−1.35737
H	−2.221345	−1.592352	−2.036752	H	−2.21836	−1.58743	−2.01763
H	−0.02437	−3.061765	0.676761	H	−0.02138	−3.05684	0.69588
H	0.83931	−0.5876	2.301652	H	0.8423	−0.58268	2.32078
H	−0.399633	−1.76372	2.813248	H	−0.39664	−1.7588	2.83237
H	1.279312	−2.268492	2.641352	H	1.2823	−2.26357	2.66048
H	2.361659	−2.329533	0.307096	H	2.36465	−2.32461	0.32622
H	1.322802	−2.140683	−1.145177	H	1.32579	−2.13576	−1.12605
H	3.190824	1.694688	0.817481	H	3.19381	1.69961	0.8366
H	2.603273	2.121036	−0.80824	H	2.60626	2.12596	−0.78912
H	4.326396	1.819222	−0.53876	H	4.32939	1.82415	−0.51964
H	4.981813	−0.424167	−1.39837	H	4.9848	−0.41924	−1.37925
H	3.792441	−1.83303	−1.332995	H	3.79543	−1.82811	−1.31387

Table C3. Theoretical (M062X/SDD) frequency analysis of product mass spectrometric ion of PPG PPG_59_a in ground and transition state obtained using the atomic co-ordinates summarised in **Table C2**.

PPG_59_a (TS)				**PPG_59_a (GS)**			
Frequencies	−59.531	161.6659	383.9378	Frequencies	119.665	158.2657	390.3571
Red.masses	1.0719	1.0393	2.1988	Red.masses	1.1009	1.0178	2.2169
Frc consts	0.0022	0.016	0.191	Frc consts	0.0093	0.015	0.199
IR Inten	2.5596	1.1818	0.1619	IR Inten	2.4473	1.5623	0.0817
Frequencies	477.8499	500.9007	754.5675	Frequencies	484.1828	505.2979	747.4988
Red. masses	2.0305	2.5918	1.1552	Red. masses	2.0678	2.5307	1.1328
Frc consts	0.2732	0.3831	0.3875	Frc consts	0.2856	0.3807	0.3729
IR Inten	6.0744	14.2064	147.6085	IR Inten	6.7769	13.7303	162.4053
Frequencies	828.636	953.7192	973.5774	Frequencies	839.0621	953.8153	986.7711
Red. masses	3.3347	1.2726	1.4897	Red. masses	3.4093	1.2811	1.4688
Frc consts	1.3491	0.682	0.8319	Frc consts	1.4142	0.6867	0.8426
IR Inten	14.3116	35.4303	18.435	IR Inten	9.8856	30.0706	13.8397
Frequencies	1092.2591	1101.7136	1141.8021	Frequencies	1097.6974	1099.8507	1144.7432
Red. masses	1.3779	1.5266	1.8357	Red. masses	1.3731	1.5186	1.8333
Frc consts	0.9685	1.0917	1.4101	Frc consts	0.9748	1.0823	1.4155
IR Inten	52.3668	119.6802	62.5486	IR Inten	51.2493	133.0399	57.1113
Frequencies	1405.9869	1427.9831	1431.4121	Frequencies	1414.7672	1428.0968	1436.661
Red. masses	1.8522	1.2331	1.28	Red. masses	1.5395	1.2288	1.405
Frc consts	2.1573	1.4815	1.5452	Frc consts	1.8156	1.4766	1.7086
IR Inten	114.1297	84.6956	219.4881	IR Inten	55.0632	210.5961	150.0326
Frequencies	1453.1923	1471.8577	1494.6666	Frequencies	1455.9467	1473.4558	1496.3859
Red. masses	1.1241	1.0696	1.1763	Red. masses	1.1935	1.0593	1.2011
Frc consts	1.3987	1.3652	1.5483	Frc consts	1.4907	1.355	1.5846
IR Inten	45.8669	6.0034	34.5566	IR Inten	60.4704	7.6949	17.2265
Frequencies	1503.7098	1620.8745	2983.38	Frequencies	1510.2023	1610.0028	3051.281
Red. masses	1.1859	3.6555	1.0603	Red. masses	1.2436	3.1837	1.0454
Frc consts	1.5799	5.6585	5.5604	Frc consts	1.6711	4.8623	5.7345
IR Inten	61.3443	105.0078	39.7293	IR Inten	78.2548	92.5827	62.9395
Frequencies	3097.4065	3121.6031	3192.7243	Frequencies	3059.4984	3143.207	3153.8604
Red. masses	1.0357	1.0789	1.0967	Red. masses	1.0451	1.0902	1.0842
Frc consts	5.8542	6.1941	6.5864	Frc consts	5.764	6.3463	6.3539
IR Inten	34.9346	11.4688	16.3165	IR Inten	27.2432	7.1108	8.42
Frequencies	3220.2439	3307.0024	3613.0497	Frequencies	3206.006	3224.9368	3629.2815
Red. masses	1.1056	1.0962	1.0683	Red. masses	1.104	1.105	1.0682
Frc consts	6.755	7.0632	8.2165	Frc consts	6.6858	6.7709	8.2897
IR Inten	4.1933	0.1105	260.4298	IR Inten	2.5904	4.4613	258.5539

Table C4. Experimental mass spectrometric measurands of sample Cell_5 over short spans of scans 3500–3514 and 3528–3531 of PPG peaks at m/z 59, 117, 175, and 233, respectively; descriptive statistics; parameters of Equation (2).

Scans	**m/z**	***I***	**m/z**	***I***	**m/z**	***I***	**m/z**	I^2
3500	59.05063	9648.11788	117.09517	13,572.8751	175.1405	7090.6324	233.09973	1.41×10^8
3501	59.05063	9184.12574	117.09517	14,595.9335	175.1405	6952.74123	233.09973	1.03×10^8
3502	59.05063	9201.11788	117.09517	13,567.8751	175.1405	6892.6324	233.09973	1.41×10^8
3503	59.05063	9362.12574	117.09517	13,066.9335	175.1405	7542.74123	233.09973	1.06×10^8
3505	59.05063	8631.12574	117.09517	13,083.9335	175.1405	6804.74123	233.09973	1.23×10^8
3506	59.05063	8992.12574	117.09517	13,546.9335	175.1405	6664.74123	233.09973	1.16×10^8
3507	59.05063	9277.12574	117.09517	13,252.9335	175.1405	6468.74123	233.09973	1.15×10^8
3508	59.05063	9107.11788	117.09517	12,792.8751	175.1405	6536.6324	233.09973	1.02×10^8
3509	59.05063	9204.12574	117.09517	13,645.9335	175.1405	6680.74123	233.09973	1.27×10^8
3510	59.05063	9788.11788	117.09517	13,160.8751	175.1405	6551.6324	233.09973	1.07×10^8
3511	59.05063	8596.12574	117.09517	12,732.9335	175.1405	6411.74123	233.09973	1.13×10^8
3512	59.05063	8606.12574	117.09517	14,161.9335	175.1405	6525.74123	233.09973	1.17×10^8
3513	59.05063	8912.11788	117.09517	13,713.8751	175.1405	6724.6324	233.09973	1.13×10^8
3514	59.05063	8583.11788	117.09517	12,658.8751	175.1405	6414.6324	233.09973	1.19×10^8
3528	59.05063	8954.11002	117.09517	14,021.8168	175.1405	5871.52358	233.09973	9.03×10^7
3529	59.05063	9212.10216	117.09517	13,226.7585	175.1405	6339.41475	233.09973	1.08×10^8
3530	59.05063	8352.11002	117.09517	13,318.8168	175.1405	6447.52358	233.09973	1.15×10^8
3531	59.05063	8296.11002	117.09517	13,639.8168	175.1405	6355.52358	233.09973	1.05×10^8
Mean	59.05063	-	117.09517	-	175.1405	-	233.09973	-
sd(yEr±)	0	-	0	-	0	-	0	-
se(yEr±)	0	-	0	-	0	-	0	-
$\langle I \rangle$	-	8994.84141	-	13,431.2182	-	6626.48388	-	10,678.9706
$\langle I \rangle^2$	-	8.09×10^7	-	1.80×10^8	-	4.39×10^7	-	1.14×10^8
$\langle I^2 \rangle$	-	8.11×10^7	-	1.81×10^8	-	4.40×10^7	-	1.14×10^8
$\langle I^2 \rangle - \langle I \rangle^2$	-	165,228.009	-	242,377.933	-	120,911.388	-	321,000
D''_{SD}	-	4.36×10^{-12}	-	6.40×10^{-12}	-	3.19×10^{-12}	-	8.47×10^{-12}